ACS OMEGA

Open Access



http://pubs.acs.org/journal/acsodf

Article

# Facile Synthesis of Natural Kaolin-Based CuO Catalyst: An Efficient Heterogeneous Catalyst for the Catalytic Reduction of 4-Nitrophenol

Zinabu Gashaw Asmare, Belete Asefa Aragaw,* and Minaleshewa Atlabachew*

Cite This: *ACS Omega* 2024, 9, 48014−48031

Read Online

ACCESS | Metrics & More | Article Recommendations | Supporting Information

**ABSTRACT:** Water contamination by nitro compounds from various industrial processes has significantly contributed to environmental pollution and severely threatened aquatic ecosystems. Inexpensive, efficient, and environmentally benign catalysts are required for the catalytic reduction of such nitro compounds. This study reports the fabrication of various nanocomposites (NCs) of copper oxide nanoparticles (CuO NPs) supported on a kaolin sheet using straightforward and simple one-pot synthesis procedures that control the metal precursor to kaolin ratios. The selected as-synthesized CuO/kaolin NC was characterized using a range of advanced spectroscopic and microscopic methods, such as X-ray diffraction (XRD), Fourier transform infrared spectroscopy (FT-IR), ultraviolet−visible (UV−vis) spectroscopy, field emission scanning electron microscopy (FE-SEM), transmission electron microscopy (TEM), energy dispersive X-ray spectroscopy (EDX), high-angle annular dark-field scanning TEM (HAADF-STEM), and $N_2$ adsorption/desorption analysis. The characterization results confirmed the successful incorporation of CuO NPs into the kaolin sheets, which had an average size of about 18.7 nm. The fabricated CuO/kaolin NC was used as a heterogeneous catalyst for the efficient reduction of 4-nitrophenol (4-NP) to 4-aminophenol (4-AP) in the presence of sodium borohydride ($NaBH_4$) in an aqueous system at room temperature. The catalyst demonstrated superior catalytic performance with high 4-NP conversion into 4-AP (>99%) in the aqueous phase (50 mL, 20 mg $L^{-1}$) within 6 min. In addition, the reaction kinetics of 4-NP reduction was also investigated, and the reaction followed the pseudo-first-order kinetics equation with the apparent rate constant of 1.76 $min^{-1}$. Furthermore, the Arrhenius and Eyring parameters for the catalytic hydrogenation reaction of 4-NP were calculated in order to investigate the catalytic reaction process in more detail. Moreover, the catalyst exhibited excellent reusability and stability over seven repeated catalytic test cycles without any noticeable decline in catalytic activity. Therefore, this paper could provide a novel, efficient, and environmentally promising clay-based non-noble metal oxide nanocatalyst to reduce nitro compounds in the aqueous system.

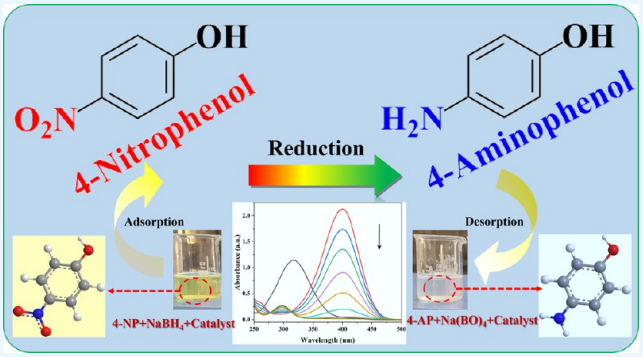


## 1. INTRODUCTION

The amount of dangerous pollutants discharged into the environment is increasing exponentially due to global population expansion as well as industrial and agricultural activity.[1] The paper and pulp, printing, textile, paint, iron-steel, pharmaceutical, pesticide, and petroleum industries are the primary sources of various organic and inorganic toxic pollutants in their industrial wastewater. These pollutants include synthetic dyestuffs, benzene, phthalates, hydrocarbons, polychlorinated biphenyls (PCBs), sulfonamides, phenols, and aromatic nitro compounds.[2] Because they are toxic and carcinogenic, they have become a key research topic for academic and industrial fields. Among these pollutants, 4-nitrophenol (4-NP) is the most harmful, nonbiodegradable, and water-soluble substance mainly released into the environment through wastewater from the pesticide, paper, dye, agrochemical, and pharmaceutical industries.[3] 4-NP has mutagenic and carcinogenic effects on human and animal health.[4,5] 4-NP is listed as a priority contaminant by the Environmental Protection Agency (EPA).[6,7] Because of its high Hammet constant (0.778), it is regarded as one of the most challenging aromatic compounds to remove using traditional oxidizing techniques.[2] It can, however, be reduced to its amino derivative, 4-aminophenol (4-AP), which is nontoxic and has a significant market value in the manufacture of numerous essential products such as plastic products, antipyretics, corrosion inhibitors in paints, acetaminophen,

Received: April 27, 2024
Revised: October 16, 2024
Accepted: November 15, 2024
Published: November 21, 2024

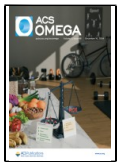

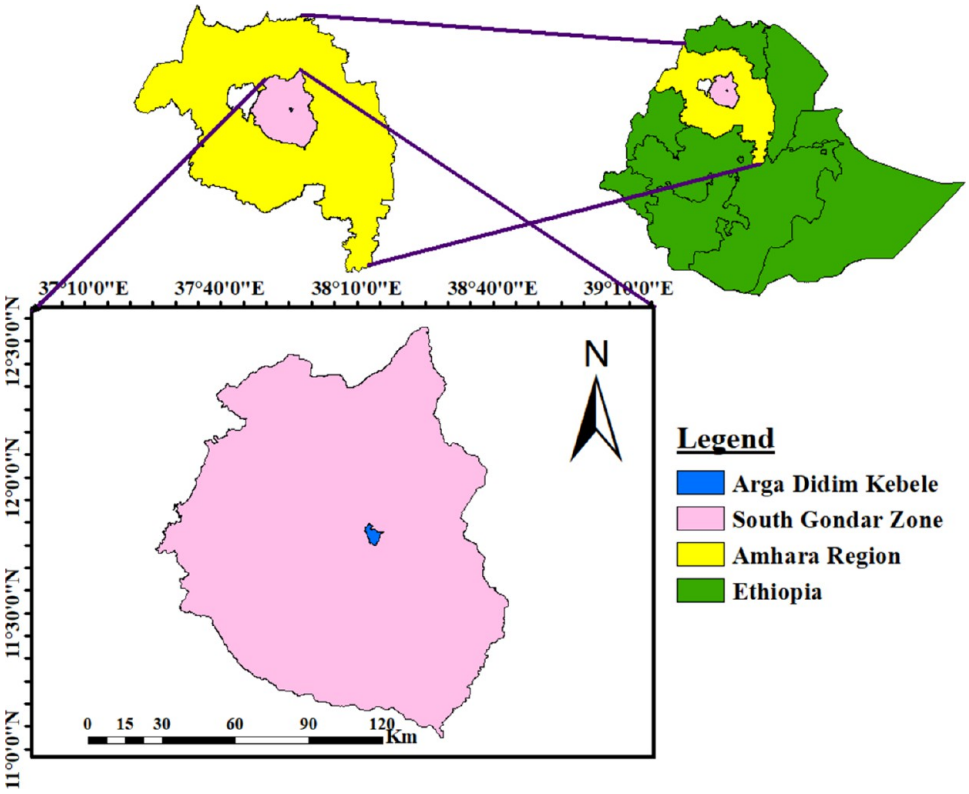


**Figure 1.** Sample location map.

anticorrosion lubricants in fuels, analgesics, paints, hair dye, and other fine chemicals.[2,8] In light of this, there has been a lot of interest in reducing 4-NP to 4-AP in recent years. The reduction process of 4-NP on nanoparticle surfaces by $NaBH_4$ has gained a lot of interest due to its practicality, effectiveness, environmental friendliness, and crucial industrial role.[9]

To date, several methods, such as electrolytic reduction, photo reduction, homogeneous and heterogeneous catalytic transfer hydrogenation, metal/acid reduction, and the use of reducing agents like hydrazine hydrates and hydrazine, have been employed for the reduction of nitrophenols to aminophenols.[10−12] Several limitations, including the need to recycle catalysts, the issue of disposing of metal oxide sludge, the carcinogenic and mutagenic properties of hydrazine, etc., made searching for alternative solutions imperative. To get rid of these harmful pollutants, scientists have been continuously investigating novel and effective techniques, as well as creating easy-to-use, environmentally friendly processes. Though thermodynamically possible, the reduction reaction of 4-NP to 4-AP by $NaBH_4$ is kinetically limited without a catalyst because of the large kinetic barrier due to the high potential difference between the mutually repulsive molecules of 4-NP (acceptor) and $BH_4^-$ (donor). Therefore, developing a cheap, efficient, and environmentally friendly catalyst for the catalytic hydrogenation of 4-NP is crucial. Among several methods, the chemical reduction of 4-NP to 4-AP catalyzed by metal (M) and metal oxide (MO) nanoparticles (NPs) has been widely studied, mainly with $NaBH_4$ as the reducing agent.[13,14]

These days, due to their diverse structures, unique features, and cutting-edge technological applications, metal oxides are undoubtedly among the functional materials that are being studied the most.[15] However, strong interactions between the oxide particles, particularly those of their nanostructured counterparts, cause the particles to clump and aggregate,[16] which lowers the relevant characteristics and makes it difficult to recover the particles from the reaction mixture for reuse. As a result, dispersing metal oxide nanoparticles across various supporting substrates, such as metal oxides,[2] carbon compounds,[17,18] zeolites,[19] and natural clay,[20] is considered a very promising strategy for avoiding interparticle aggregation. Numerous drawbacks of the aggregation of metals and metal oxides could also be addressed by dispersing the active particles into host materials that are polymeric or biopolymeric in the right way.[21] Unfortunately, most support materials are costly, and the synthesis processes are complex and time-consuming.

Kaolin, a widely used natural clay mineral, has been explored as a nanoparticle carrier because of its low cost, abundance, and environmental friendliness.[22−24] Specifically, its remarkable characteristics, such as excellent versatility and mechanical and thermal stability, make it indispensable for serving as a support for nanocatalysts.[22] Kaolin is a type of phyllosilicate material that has been characterized by its layered structure. Because of its layered structure, transparent, nontoxic, smooth surfaces, and structural stability, two-dimensional hexagonal kaolin, kaolinite is a key component with the theoretical formula $Al_2Si_2O_5(OH)_4$, is readily adaptable to create composites and hybrids as well as a strong support substrate. The two-dimensional supports are the most desirable of these different substrates since they offer a surface on which the particles can be attached and give the bare particle surface highly active sites.[25] Li and co-workers have effectively coloaded $TiO_2$ nanoparticles and core−shell Bi-containing spheres on kaolin substrate as a highly effective photocatalyst for the degradation of methyl orange.[26] In addition to the recent advancements in kaolin nanosheet stabilization and


https://doi.org/10.1021/acsomega.4c04029
ACS Omega 2024, 9, 48014−48031

exfoliation,[27] considerable attempts have been made to integrate kaolin nanosheets with other materials, primarily focusing on noble metal nanoparticles.[28,29] It would be highly desirable to develop simple and efficient techniques for dispersing the functional metal oxide NPs throughout the kaolin nanolayer, both from the perspective of fundamental science and technological applications. Specifically, cupric oxide (CuO) is a well-known functional material that has been the subject of extensive research due to its potential uses in lithium-ion batteries, gas sensors, biocides, solar energy photovoltaics, gas sensors, and catalysis.[30,31] The CuxO clusters containing Cu(II), especially arranged on the surfaces of $TiO_2$, provide antibacterial characteristics and effective visible-light photooxidation of volatile organic compounds to the resultant composites.[32,33] Furthermore, dispersing CuO particles on the graphene oxide can improve activity and stability.[34] In other studies, noble metal nanoparticles have successfully dispersed into the beneficiated kaolin to remove organic pollutants from wastewater.[22,23,35]

We recently synthesized silver NPs supported on kaolin clay by a facile adsorption-reduction method for the catalytic reduction of methylene blue dye in an aqueous medium.[35] In this work, we explain CuO NPs that are firmly attached to the kaolin surface, which was treated through the wet beneficiation process. The as-synthesized CuO/kaolin NC catalytic performance was examined by converting 4-NP to 4-AP with $NaBH_4$, exhibiting excellent reduction performance. The catalytic performance of the CuO/kaolin NC catalyst was also thoroughly investigated by changing the CuO loadings. Moreover, after seven recycling processes, there was a slight decrease in the catalytic activity of the catalyst to reduce 4-NP, indicating that it was very stable for long-term reuse. This kaolin-based metal oxide catalyst demonstrates that the material is a promising environmental catalyst for practical application in wastewater treatment due to its facile preparation method, high catalytic performances toward the reduction of 4-NP, mild reaction conditions, and stable reusability. Thus, this work would extend the applications of kaolin and motivate other researchers to investigate more of this promising clay material in other catalytic systems as catalyst support.

## 2. MATERIALS AND METHODS

**2.1. Materials.** The raw kaolin clay mineral sample was taken from a deposit in the South Gondar Zone of Arga Didim Local Government Area, Ethiopia (Figure 1), which was utilized in this work as a robust and solid support for the CuO NPs. The clay mineral was allowed to completely dry in the laboratory at room temperature (~22 °C). The analytical grade reagents included copper sulfate pentahydrate ($CuSO_4 \cdot 5H_2O$, 99.99%, Unichem chemical), sodium hydroxide (NaOH, 98%, Unichem chemical), sodium borohydride ($NaBH_4$, 97%, Savgan Heights plc), and 4-nitrophenol (4-NP, $C_6H_5NO_3$, Sigma-Aldrich), which were used exactly as supplied. All the solutions were made with deionized (DI) water.

**2.2. Methods.** *2.2.1. Wet Beneficiation Treatment of Raw Kaolin Clay.* Prior to utilization, the raw kaolin clay sample was ground into a fine powder with a mortar and pestle. The mixture was further sieved using a 75 $\mu$m sieve to eliminate any residual coarse particles and was then stored. To produce pure and fine powder, the wet beneficiation process is applied to remove chemical and physical impurities, such as soluble salts, metallic oxide, organic debris, quartz, grits, and typically coarse particles.[24,35,36] To do this, 100 g of powdered kaolin were soaked in 1 L of DI water and stirred for 24 h at room temperature. After settling, the mixture produced a firm clay cake, which was filtered out and washed several times with DI water. After that, the solid product was subsequently dried overnight at 60 °C in an air oven. Lastly, the dried product was thoroughly pulverized, sieved, and kept before being used and analyzed further.

*2.2.2. Synthesis of CuO NPs and CuO/Kaolin Nanocomposites.* The CuO/kaolin nanocomposite catalysts with various CuO NP loadings were prepared by simple wet precipitation followed by calcination. In a typical experiment, 0.5 g of $CuSO_4 \cdot 5H_2O$ was dissolved in 100 mL of DI water and stirred for 10 min on a hot plate to get a homogeneous, blue-colored solution. After adding beneficiated kaolin clay powder (1 g) to the precursor solution, it was vigorously stirred for 1 h. NaOH solution (0.5 M) was added in drops to the mixture to adjust the pH to around 12 under stirring at 60 °C for 1 h. The formed heterogeneous gel was allowed to age overnight at ambient temperature. After aging, the mixture was separated and rinsed thoroughly with DI water until the filtrate solution turned neutral. The final products were ground into a fine powder after overnight drying at 80 °C in an electric oven. Finally, the powder sample was calcined at 500 °C in a furnace under air for 3 h. To observe the effect of the metal precursor amount, the mass of $CuSO_4 \cdot 5H_2O$ was varied from 0.25 to 1.5 g by keeping the mass of kaolin at 1 g. These catalysts were labeled as CuO/kaolin NC-$X$ ($X$ = 0.25, 0.5, 1, and 1.5) based on the various mass ratios of $CuSO_4 \cdot 5H_2O$ to beneficiated kaolin clay.

A similar procedure was used to synthesize CuO/kaolin nanocomposites to synthesize unsupported CuO NPs, except that kaolin was absent in the reaction mixture.

*2.2.3. Material Characterization.* The ultraviolet−visible (UV−vis) absorption spectra of samples were obtained using a DR6000 UV−vis spectrophotometer (Cole-Parmer, Hach Company) at room temperature. Fourier transform infrared spectroscopy (FT-IR) spectra of the samples were recorded over the wavenumber range of 4000−400 $cm^{-1}$ with 4 $cm^{-1}$ resolution using an FT/IR-6600 spectrometer (JASCO., Japan), using the KBr disk method. The morphology, elemental composition, and dispersion pattern of the prepared nanoparticles were examined on a field emission-scanning electron microscope (FE-SEM) equipped with an energy-dispersive X-ray spectrometer (EDX) (ZEISS SIGMA), and SEM images were obtained by a JEOL NeoScope JCM-6000 Plus Benchtop apparatus at a 10 kV accelerating voltage operating condition. Transmission electron microscopy (TEM) and high-angle annular dark-field scanning TEM (HAADF-STEM) images were obtained on a JEOL JEM-2100F transmission electron microscope using an accelerating voltage of 200 kV. Note that the STEM system was equipped with energy-dispersive X-ray spectroscopy (EDX) units. Powder X-ray diffraction (XRD) patterns of the as-prepared samples were obtained on a Shimadzu XRD-7000 diffractometer using a Cu K$\alpha$ radiation source ($\lambda$ = 1.5406 Å) running at 40 kV and 30 mA in the 2$\theta$ degree range from 10 to 80° at a scan rate of 3° $min^{-1}$. Using a Quantachrome AsiQwin Automated Gas Sorption System, nitrogen adsorption and desorption isotherms at 77 K were recorded. The investigation of surface area and pore-size distribution was carried out by


https://doi.org/10.1021/acsomega.4c04029
ACS Omega 2024, 9, 48014−48031

Brunauer–Emmett–Teller (BET) and density functional theory (DFT) calculations, respectively.

*2.2.4. Catalytic Reduction of 4-NP.* To assess the catalytic performance of the CuO/kaolin NC, the reduction of 4-NP with excess $NaBH_4$ was selected as a model reaction. Initially, an aqueous 4-NP solution (50 mL, 20 mg $L^{-1}$) was mixed with 0.132 mmol of $NaBH_4$ (5 mg), forming a deep yellow 4-nitrophenolate solution. Subsequently, 5 mg of the synthesized CuO/kaolin NC was added with constant stirring at room temperature. From the time of catalyst addition, a few portions of 4-NP samples were collected at definite time intervals, and the change in absorbance was measured using a UV–vis spectrophotometer within the 250–500 nm scanning range. All the spectra were normalized by using OriginPro 2024 software. From the UV–vis absorption spectra, the reduction efficiency of 4-NP was calculated using eq 1

$$\text{reduction}\ (\%) = \frac{(A_0 - A_t)}{A_0} \times 100\% \quad (1)$$

where $A_0$ and $A_t$ are absorbances of 4-NP aqueous solution at initial and time $t$, respectively, in the reaction mixture.

The kinetic equation for the catalytic reduction of 4-NP to 4-AP by $NaBH_4$ over CuO/kaolin NC in aqueous solution can be written by applying the linear equation of the pseudo-first-order (PFO) model (eq 2)

$$\ln\left(\frac{A_t}{A_0}\right) = -k_{app}t \quad (2)$$

where $k_{app}$ is the apparent rate constant. The study investigated the effects of several factors on the efficiency of the fabricated catalyst, including reaction temperature, catalyst dose, $NaBH_4$ amount, and initial 4-NP concentration.

*2.2.5. Reusability of CuO/Kaolin Nanocomposite.* The catalytic performance of the CuO/kaolin nanocomposite was assessed over multiple cycles to evaluate its reusability. The experiments were conducted using the exact stoichiometry of the mixture used for the original tests. In the first cycle, 10 mg of CuO/kaolin NC was added to the mixture of 15 mL of 4-NP aqueous solution (50 mg $L^{-1}$) and 0.264 mmol of $NaBH_4$ (10 mg). After 5 min of stirring the mixture, the CuO/kaolin NC was separated by centrifugation at 4000 rpm for 10 min and rinsed thoroughly with DI water to remove any adsorbed compounds before being used in the next catalytic cycle. The same procedure was carried out for the subsequent six runs.

## 3. RESULTS AND DISCUSSION

**3.1. Synthesis of CuO/Kaolin Nanocomposites.** The overall synthesis procedure of the CuO/kaolin NCs is illustrated in Scheme 1. The $Cu^{2+}$ ions become adsorbed in the pores of a cross-linked network of kaolin from the bulk region in the basic medium due to the formation of a dative bond. The $Cu^{2+}$ ions on the surface of kaolin precipitated as $Cu(OH)_2$ after addition of base, NaOH. $Cu(OH)_2$ is converted to CuO NPs upon calcination, and the kaolin is changed into amorphous metakaolin.[37] Hydrous kaolin's distinguishing features include its tiny particle size, plate-like or lamellar particle form, and chemical inertness. Calcined kaolin (metakaolin) is an anhydrous aluminum silicate produced by heating natural kaolin to high temperatures. When structural water is removed by dehydroxylation, the aluminum migrates into empty spaces created by the interlayer spacing, causing distortion or buckling in the 1:1 Al–Si layers.

**Scheme 1. Pictorial Diagram of Synthesis of CuO/Kaolin NC**

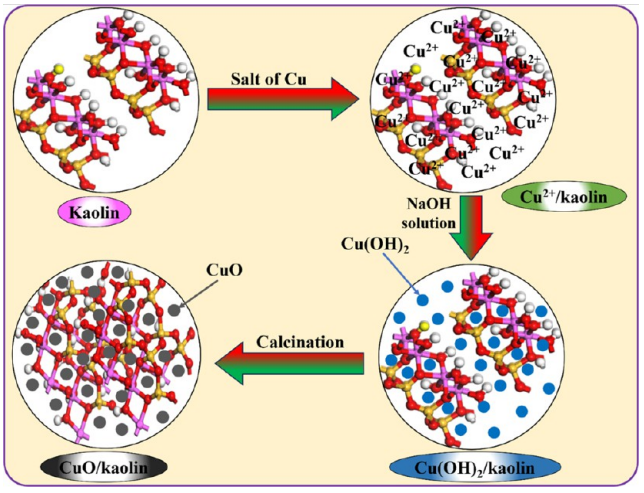


The transformation of kaolin into metakaolin is characterized by removing the chemically bonded water and breaking the hydroxyl bonds. At higher temperatures, metakaolin is formed by dehydroxylation of the structure of the Al–OH and Si–OH groups of kaolin, as shown in eq 3.[38]

$$Al_2Si_2O_5(OH)_4 \xrightarrow{450-700\ ^\circ C} (Al_2O_3{\cdot}2SiO_2) + 2(H_2O)\uparrow \quad (3)$$

The structural change is characterized by a loss of crystallinity (Figure 6B) and an accompanying shift in aluminum coordination from octahedral to tetrahedral. The color of the powder changed from light black to brownish-black when the ratio of $CuSO_4{\cdot}5H_2O$ to kaolin increased from 0.25 to 1.5, which implied that different sizes of CuO NPs with increased numbers were immobilized on the surface of kaolin layers. The 2D structure of kaolin is shown in Figure S1 in the Supporting Information.

**3.2. Characterization of the CuO/Kaolin Nanocomposite.** The absorbances of diluted kaolin and CuO/kaolin NC-1 dispersions were recorded with a UV–vis spectrophotometer at room temperature (Figure 2A). The kaolin dispersion showed no clear peak, while a clear peak at around 364 nm was observed for CuO/kaolin NC-1 dispersion. This peak is a result of the electronic transition of CuO NPs deposited on kaolin sheets from the valence band to the conduction band. The spectra confirmed the presence of CuO NPs in kaolin surfaces.[39]

The chemical functional group of kaolin, calcined kaolin, and the as-prepared CuO/kaolin NC-1 were subjected to FT-IR analysis; the data is shown in Figure 2B. The distinctive peaks of kaolin were detected at 1035 and 1624 $cm^{-1}$, which are ascribed to the deformation of water molecules and the in-plane stretching vibration of the Si–O (O–Si–O and Si–O–Si) network, respectively. In addition, the vibrations of perpendicular Si–O stretching, Al–O–Si deformation, and Si–O–Si deformation are correlated with the maxima at 685, 538, and 464 $cm^{-1}$. Furthermore, the O–H deformation vibration of internal hydroxyl groups and Si–O–Si in-plane stretching indexed at 909 $cm^{-1}$. Although an organic impurity is present, it is negligible due to beneficiation, as indicated by the very weak peak at 2920 $cm^{-1}$ from the raw kaolin-attributed aliphatic hydrocarbon (CH) stretching. The FTIR


https://doi.org/10.1021/acsomega.4c04029
ACS Omega 2024, 9, 48014–48031

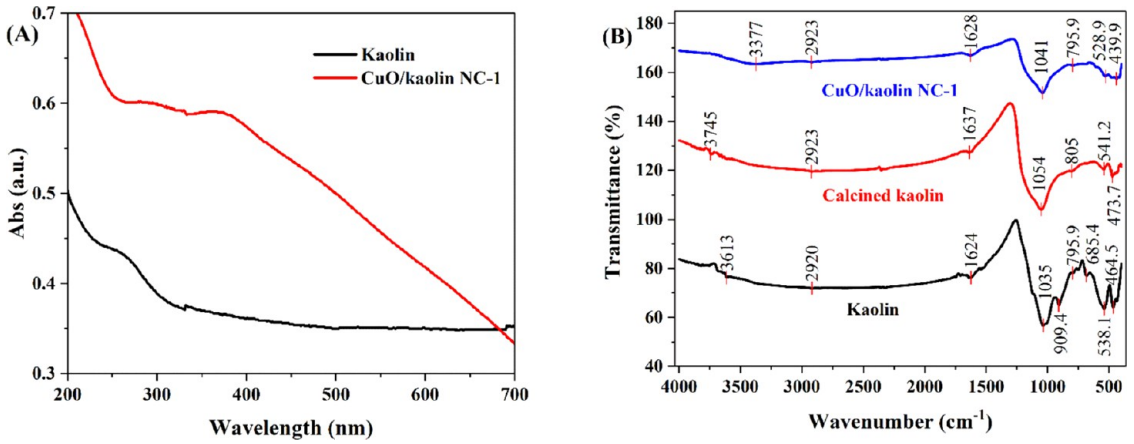


**Figure 2.** (A) UV−vis absorption spectra of kaolin and CuO/kaolin NC-1. (B) The FT-IR spectra of kaolin, calcined kaolin, and CuO/kaolin NC-1.

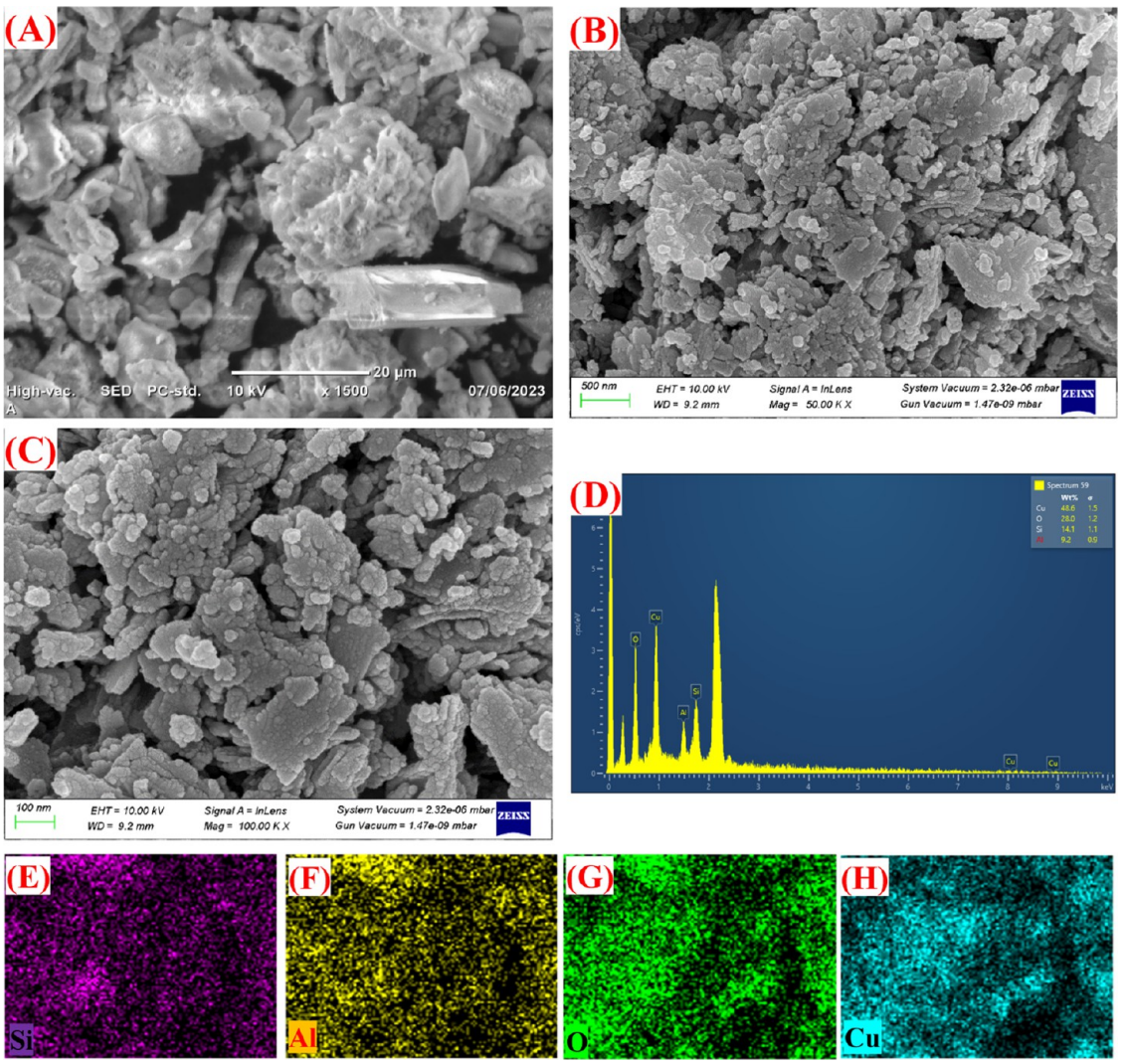


**Figure 3.** (A) FE-SEM images of kaolin. (B, C) The FE-SEM images of CuO/kaolin NC-1 at various magnifications. (D) The EDX spectrum of CuO/kaolin NC-1. (E−H) Elemental mapping images of CuO/kaolin NC-1.

spectrum of kaolin also exhibits a peak at 3613 $cm^{-1}$, which is indicative of the asymmetric stretching of the O−H group.[40] The FT-IR spectrum of CuO/kaolin NC-1 shows peaks at 439.9 and 528.9 $cm^{-1}$, revealing the deposition of CuO NPs on the kaolin's surface.[41] Additionally, the nanocomposite showed a distinctively high absorbance at 1041 $cm^{-1}$, connected to CuO's Cu−O bending vibration, in line with other findings.[42] The Cu−O bond rocking out of the plane at 1628 $cm^{-1}$ was another way to identify CuO NPs. The stretching vibration of the hydroxyl group from the leftover water is represented by


https://doi.org/10.1021/acsomega.4c04029
ACS Omega 2024, 9, 48014−48031

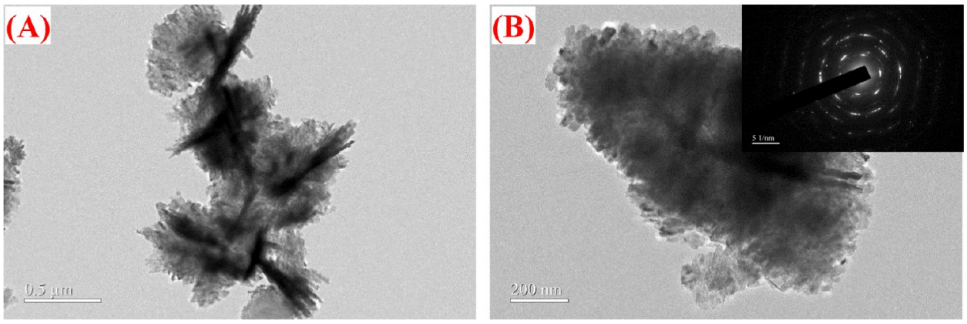


**Figure 4.** TEM images of CuO/kaolin NC-1 with different magnification: (A) 500 nm and (B) 200 nm. The inset in (B) is SAED pattern of CuO NPs.

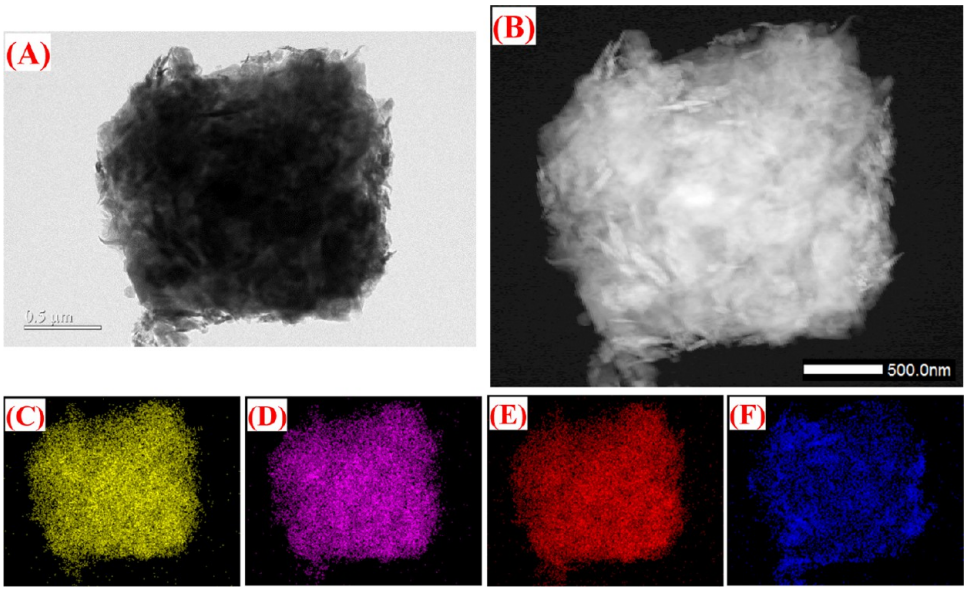


**Figure 5.** TEM (A) and HAADF-STEM (B) images of CuO/kaolin NC-1. EDX elemental mapping images of Si (C), Al (D), O (E) and Cu (F).

the peak at 3377 $cm^{-1}$. All spectra also contain a band at 795.9, 805, and 795.9 $cm^{-1}$ in kaolin, calcined kaolin, and CuO/kaolin NC-1, respectively, attributed to symmetrical Si−O stretching vibrations of quartz. Compared to pure kaolin, many peaks disappear in the CuO/kaolin NC, indicating that the kaolin's crystallinity changed into an amorphous phase due to the calcination process.[37]

The surface morphologies of kaolin and CuO/kaolin NC-1 samples were investigated by SEM measurements (Figure 3A−C). The particle size distribution of kaolin was not uniform, with smaller particles able to form bigger aggregates dispersed on the outside and the surface of larger particles, as demonstrated in Figure 3A. The smooth kaolin flakes had become rough and porous following the calcination and deposition of CuO NPs (Figures 3B,C and S2A), confirming the deposition of CuO NPs on the surface of kaolin sheets. In the images, the CuO NPs are seen as bright, nearly uniform spherical dots immobilized on the surface of kaolin with an average diameter of 22.26 ± 5.09 nm (Figure S2B). Furthermore, FE-SEM images (Figure 3C) clearly show the uniform loadings and nonagglomerated CuO NPs on the kaolin support, demonstrating the support's importance in reducing CuO NP aggregation on the kaolin's surface. This strengthens the fact that the copper cation is uniformly distributed on the surface of kaolin due to the electrostatic interaction between the copper cation and the negative surface charge of the kaolin, after which it is converted to $Cu(OH)_2$ and CuO. The elemental composition of CuO/kaolin NC-1 was investigated by EDX analysis, and the result is shown in Figure 3D. The EDX spectrum confirmed that Si, Al, Cu, and O are the sole elements (other than H) in the composite CuO/kaolin NC-1. EDX elemental mapping also confirmed the uniform distribution of the Cu element on the kaolin's surface (Figure 3H).

The detailed structure and interfacial feature of the CuO/kaolin NC-1 were further examined by TEM and are shown in Figure 4A,B. Several CuO/kaolin nanoleaves with uniformly sized multiple petals were observed. No other morphology of pure kaolin or CuO NPs coincides with the TEM images of the nanoleaves, showing their excellent homogeneity. The inset image of Figure 4B, which displays the selected area electron diffraction (SAED) pattern of a single CuO NP, indicated that the monoclinic CuO NPs that were generated are composed of single crystal structures. Moreover, high-angle annular dark-field scanning transmission electron microscopy (HAADF-STEM) imaging and EDX elemental mapping of the TEM picture in Figure 5A have confirmed the structural characteristics of the representative CuO/kaolin NC-1, as illustrated in Figure 5B. The existence of various elements within the CuO/kaolin NC-1 is responsible for the color points, as illustrated in Figure 5C−F. The Si and Al elements are present due to the kaolin substrate. Si, Al, O, and Cu elements in the sample are


https://doi.org/10.1021/acsomega.4c04029
ACS Omega 2024, 9, 48014−48031

uniformly distributed over the nanocomposite. The homogeneous distribution of Cu on the surface of the kaolin substrate can be observed in Figure 5F.

A powder X-ray diffractometer was used to examine the phase purity and degree of crystallinity of kaolin and CuO/kaolin NC-1 (Figure 6). The diffraction peaks of beneficiated

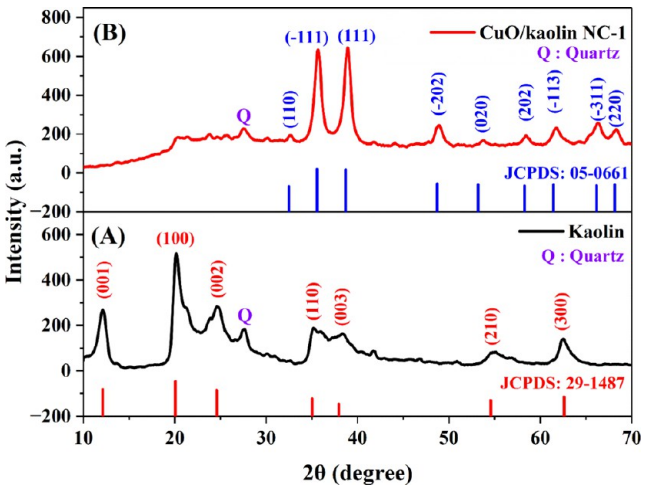


**Figure 6.** XRD patterns of (A) beneficiated kaolin and (B) CuO/kaolin NC-1 with their respective standard JCPDS data.

kaolin (Figure 6A) obtained at 2$\theta$ values of 12.12, 20.14, 24.7, 35.14, 38.42, 54.84, and 62.5° correspond to the (001), (100), (002), (110), (003), (210) and (300) planes, respectively (JCPDS 00−029−1487).[40] Additionally, according to JCPDS 5−0490, the diffraction peak at 2$\theta$ = 27.59° demonstrated the presence of quartz,[23] which is highly crystalline $SiO_2$.[37] The XRD analysis of CuO/kaolin NC-1 (Figure 6B) revealed well-defined diffraction peaks at 2$\theta$ values of 32.64, 35.74, 38.89, 48.89, 53.68, 58.44, 61.58, 66.30, and 68.31°, which correspond to the (110), ($\bar{1}$11), (111), ($\bar{2}$02), (020), (202), ($\bar{1}$13), ($\bar{3}$11) and (220) planes of monoclinic CuO, respectively, confirming the formation of CuO NPs on the kaolin surface.[43] Each of the distinctive diffraction peaks of the CuO/kaolin NC-1 sample is in good agreement with the standard CuO crystallographic data (JCPDS No. 05−0661, space group $C2/c$). The positions of all the characteristics of the XRD peaks are in agreement with the results reported previously.[43−47] CuO crystals are made easier to form when kaolin undergoes a structural change from its crystalline form to the amorphous metakaolin phase during calcination at 500 °C. The presence of the amorphous phase is confirmed by the large peak seen in the metakaolin diffraction peak at about 2$\theta$ = 15−35°.[37] Moreover, the diffraction peak at 27.51° is assigned to quartz from metakaolin.[48] The development of a pure phase CuO is indicated by the absence of any characteristic peaks of other impurities, such as $Cu(OH)_2$, $Cu_2O$, or precursors utilized.[49] The average crystallite size ($D_{hkl}$) for CuO NPs was also calculated using Scherrer's formula (eq 4).

$$D_{hkl} = \frac{0.9\lambda}{\beta_{hkl}\cos\theta} \tag{4}$$

where $\lambda$ is the wavelength of the X-ray source (1.5405 Å), $\beta$ is the full width at half-maximum (fwhm) of the diffraction peaks, and $\theta$ is the diffraction angle. The mean crystallite size of CuO NPs in the as-synthesized nanocomposite was determined to be about 18.7 nm, which is in close agreement with the values found from FE-SEM images.

Figure 7A displays the mesopore size distribution and $N_2$ adsorption and desorption isotherms for the kaolin and CuO/kaolin NC-1. Type IV isotherms with $H_3$-type hysteresis loops were seen in the $N_2$ adsorption and desorption isotherms. Mesopore capillary condensation is associated with the type IV isotherm, and slit-shaped pores are characterized by the $H_3$-type hysteresis loop.[50] Figure 7B shows the pore size distribution of kaolin and CuO/kaolin NC-1. As shown in the figure, the pore size distribution of kaolin was found in the mesopore range of 2−10 nm. Conversely, following the loading of CuO NPs onto the kaolin sheet, the proportion of mesopores increased after CuO NPs were loaded on the kaolin surface. This could be explained by the calcination of kaolin.[51]

$N_2$ adsorption and desorption isotherms were also used to investigate the texture properties of kaolin and CuO/kaolin NC-1, which are presented in Table 1. Kaolin's pore volume was 0.170 cc/g, and its $S_{BET}$ was 63.9 $m^2\ g^{-1}$. The $S_{BET}$ dropped to 46.8 $m^2\ g^{-1}$ and pore volume increased to 0.198 cc $g^{-1}$ following the loading of CuO NPs onto the kaolin surface. Furthermore, it was discovered that the average pore size of

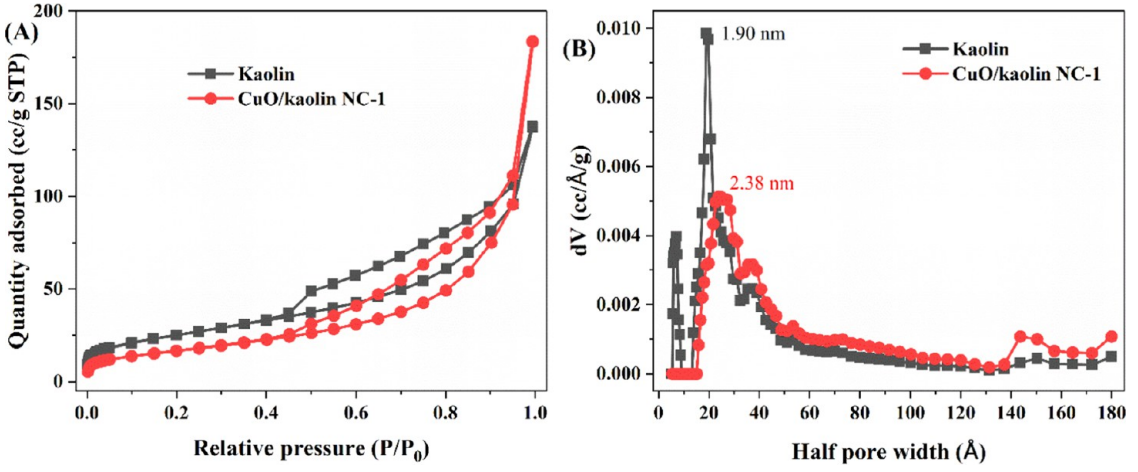


**Figure 7.** (A) $N_2$ adsorption and desorption isotherms and (B) DFT pore size distributions of kaolin and CuO/kaolin NC-1.



https://doi.org/10.1021/acsomega.4c04029
ACS Omega 2024, 9, 48014−48031

**Table 1. Textural Properties of Kaolin and CuO/Kaolin NC-1**

| sample | $S_{BET}$ ($m^2$ $g^{-1}$) | pore size (nm) | pore volume (cc $g^{-1}$) |
|---|---|---|---|
| Kaolin | 63.9 | 3.8 | 0.17 |
| CuO/kaolin NC-1 | 46.8 | 4.76 | 0.198 |

CuO/kaolin NC-1 was approximately 4.76 nm, which was comparatively higher than the 3.8 nm pore size of kaolin. The findings suggest that CuO NPs may be able to fill some tiny pores.[52]

**3.3. Catalytic Performance.** The model reaction utilized to assess the catalytic activity of the synthesized CuO/kaolin NC is the catalytic reduction of 4-NP to 4-AP in the presence of $NaBH_4$. For this purpose, 50 mL (20 mg $L^{-1}$) of 4-NP (model pollutant), 0.132 mmol (5 mg) of $NaBH_4$ (reductant), and 5 mg of CuO/kaolin NC-1 (catalyst) were mixed in a beaker under continuous stirring. After that, the volume of the reaction solution was taken at predetermined time intervals, and its UV−vis absorption spectra in the region of 250−500 nm were recorded to monitor the progress of the reaction. As shown in Figure S3A, the 4-NP shows an absorption peak at 317 nm. When $NaBH_4$ is added, the OH group of 4-NP is deprotonated, which causes the absorption peak to shift to 400 nm, which indicates the formation of a 4-nitrophenolate ion (Figure S3A).[53] Meanwhile, the light-yellow solution of 4-NP turned to deep yellow (inset image of Figure S3A). According to reports, $BH_4^-$ and 4-nitrophenolate ions are repulsive to one another. However, metal oxide nanoparticles can speed up the reduction of 4-NP by enhancing the transfer of hydrides from $BH_4^-$ to the $-NO_2$ group.[54] As the reaction continued, the intensity of the absorption peak at 400 nm rapidly decreased and eventually disappeared within 6 min, while a new absorption peak at 300 nm appeared (Figure 8A), attributed to the formation of 4-AP.[55] The isosbestic point at 277 and 314 nm (shown by ellipses in Figure 8A) also confirmed the reduction product was 4-AP and suggested no byproduct was generated during the reduction process.[56] Furthermore, the color of the 4-NP solution quickly changed from a deep yellow to a colorless state (inset image of Figure 8A), indicating the strong catalytic effectiveness of CuO/kaolin NC-1 for 4-NP reduction by $NaBH_4$. For comparison, the catalytic activity of CuO NPs in the reduction of 4-NP by $NaBH_4$ was investigated (Figure 8B). The result showed poor catalytic performance compared to CuO/kaolin NC-1 and could not be completely reduced within 10 min. As shown in Figure 8C, CuO/kaolin NC-1 performs much better than CuO NPs, indicating the catalytic activity of CuO NPs enhanced by the support kaolin. Some controlled experiments were conducted to confirm and identify the true catalyst. Under the same conditions, the 4-NP reduction reaction by $NaBH_4$ was performed without any catalyst (Figure S3B) and with the presence of beneficiated

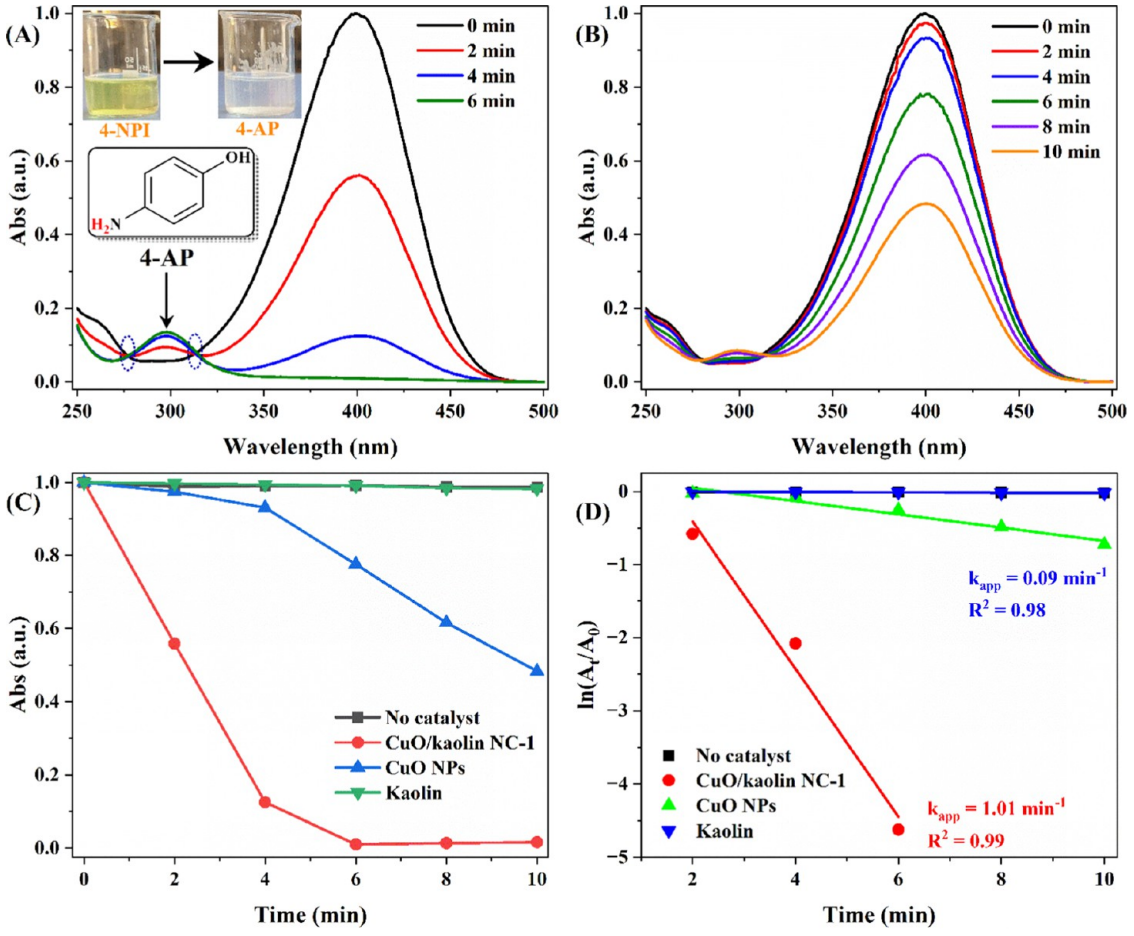


**Figure 8.** UV−vis time-dependent absorption spectra changes of 4-NP reduction using (A) CuO/kaolin NC-1 and (B) CuO NPs. (C) The plots of absorbance against reaction time. (D) The corresponding plots of $\ln(A_t/A_0)$ against reaction time. Reaction conditions: 20 mg $L^{-1}$, 50 mL of 4-NP; 0.132 mmol $NaBH_4$; 5 mg catalyst; 22 °C. Note: 4-NPI is 4-nitrophenolate ion.



https://doi.org/10.1021/acsomega.4c04029
ACS Omega 2024, 9, 48014−48031

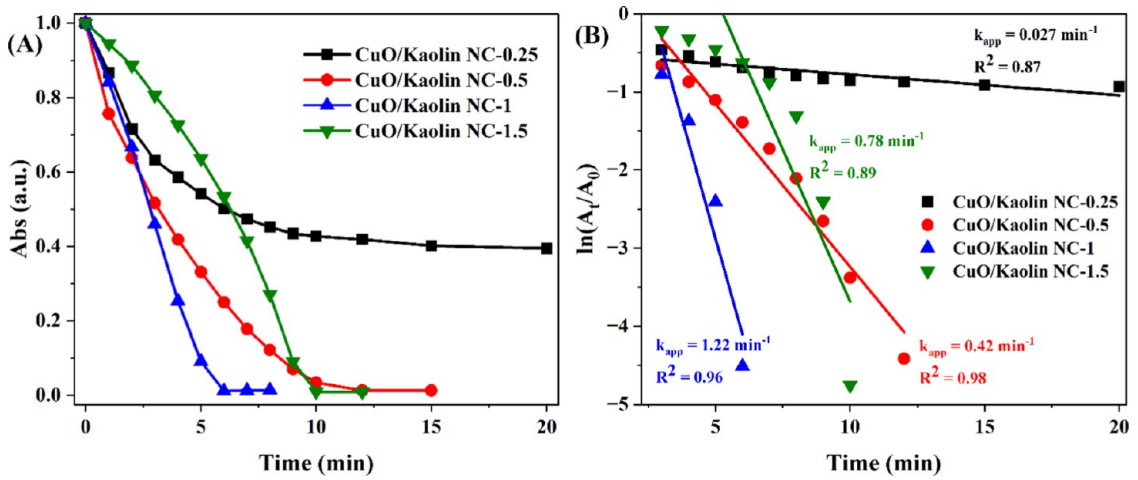


**Figure 9.** (A) Plots of absorbance against reaction time for the reduction 4-NP using various nanocomposites. (B) The corresponding plots of $\ln(A_t/A_0)$ against reaction time for the reduction of 4-NP over various nanocomposites. Reaction conditions: 20 mg $L^{-1}$, 50 mL of 4-NP; 0.132 mmol $NaBH_4$; 5 mg catalyst; 22 °C.

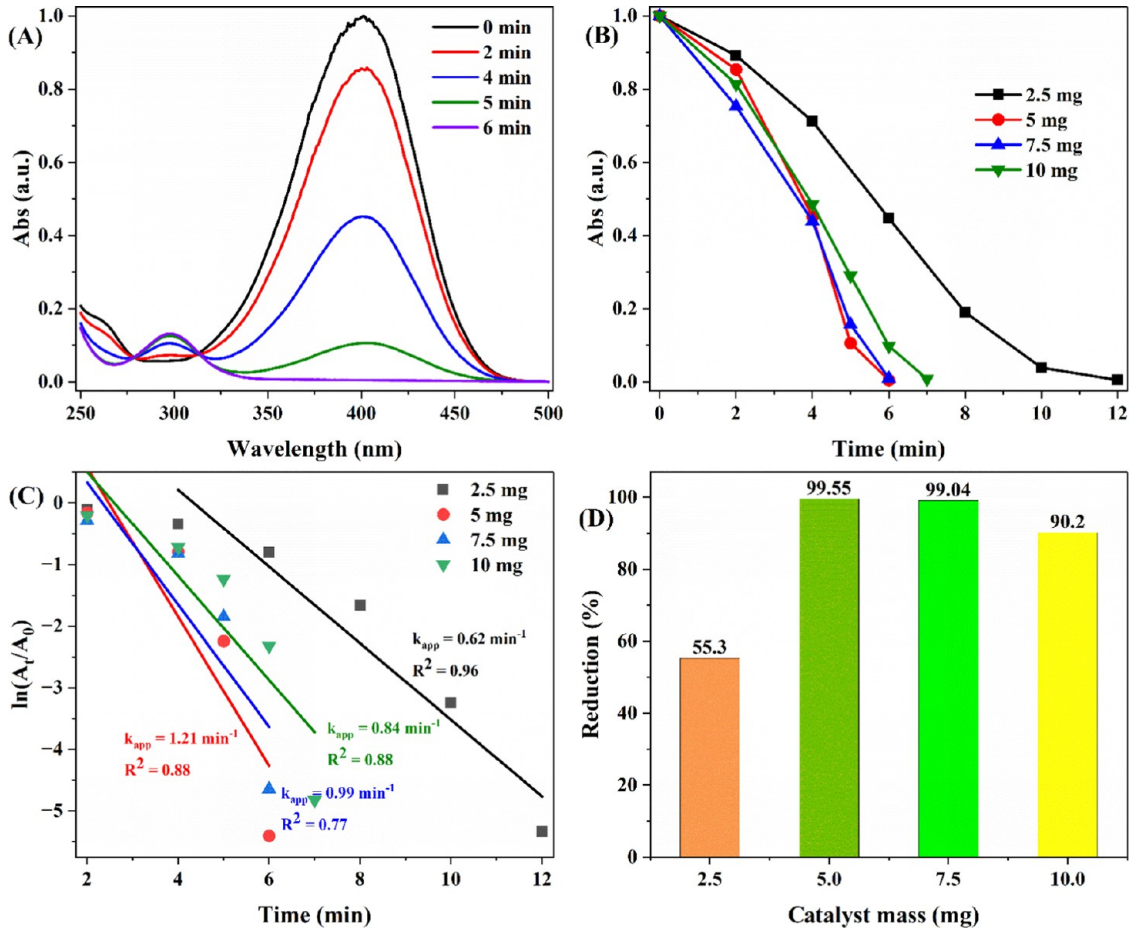


**Figure 10.** (A) UV−vis absorption spectra changes of 4-NP reduction using 5 mg CuO/kaolin NC-1. (B) The plots of absorbance against reaction time for the reduction of 4-NP using various catalyst doses. (C) The corresponding plots of $\ln(A_t/A_0)$ against reaction time. (D) Reduction of 4-NP over various 4-NP concentrations within 6 min reaction time. Reaction conditions: 20 mg $L^{-1}$, 50 mL of 4-NP; 0.132 mmol $NaBH_4$; 22 °C.

kaolin (Figure S3C). No significant absorption spectra change of the 4-nitrophenolate ion were observed in these cases. All these results indicated that CuO/kaolin NC-1 was the true catalyst. The greater catalytic reduction efficiency of CuO/kaolin NC-1 was illustrated by plotting the reduction rate against reaction time (Figure S3D), as determined by the corresponding absorbance at 400 nm. This further demonstrates the differences in the catalytic efficiencies of the four samples. As shown in Figure 8D, good linear correlations of $\ln(A_t/A_0)$ against reaction time were obtained for CuO/kaolin NC-1 and CuO NPs, confirming the 4-NP reduction followed a pseudo-first-order kinetics. The apparent rate constant ($k_{app}$)


https://doi.org/10.1021/acsomega.4c04029
ACS Omega 2024, 9, 48014−48031

of 4-NP reduction by $NaBH_4$ over CuO/kaolin NC-1 was calculated from the slope of $\ln(A_t/A_0)$ versus reaction time plot and found to be 1.01 $min^{-1}$ with $R^2$ = 0.99, which is 11 times higher than bare CuO NPs with a $k_{app}$ of 0.09 $min^{-1}$ with $R^2$ = 0.98 (Figure 8D).

**3.4. Effect of CuO NPs Loading on Kaolin Surface.** The loading amount of CuO NPs on kaolin sheets could influence the catalytic activity of the reduction of nitroarenes. The CuO/kaolin NCs with different CuO loading amounts (CuO/kaolin NC−0.25, 0.5, 1, and 1.5, obtained using copper sulfate pentahydrate to kaolin mass ratios of 0.25, 0.5, 1, and 1.5, respectively) were prepared to study their effect on the reduction of 4-NP by $NaBH_4$. The reduction reaction efficiency of 4-NP increased with the copper sulfate pentahydrate to kaolin mass ratio increasing from 0.25 to 1 (Figure 9A). This could be attributed to the increased number of CuO NPs, which, in turn, leads to an increased specific surface area for the nanocomposite. However, when the ratio further increased to 1.5, the removal efficiency of 4-NP decreased (Figure 9A). This decline might be caused by the increase in the size of CuO NPs, owing mainly to their aggregation at overload. $NaBH_4$ almost entirely reduced 4-NP in the presence of CuO/kaolin NC-0.5, CuO/kaolin NC-1, and CuO/kaolin NC-1.5 after 12 min (Figures S4B), 6 min (Figures S4C), and 10 min (Figure S4D) exposure times, respectively. For CuO/kaolin NC−0.25, the reduction of 4−NP was slow, and there was no completion of the reaction even after 20 min of reaction time (Figure S4A). The corresponding plots of $\ln(A_t/A_0)$ versus reaction time during the reaction progress are shown in Figure 9B. The reduction efficiency of 4-NP over the reduction progress using various nanocomposites is shown in Figure S4E. CuO/kaolin NC-1 achieved 98.9% of 4-NP conversion in just 6 min, while CuO/kaolin NC-0.25, 0.5, and 1.5 are only 49.8, 75.08, and 46.64%, respectively (Figure S4F). Therefore, the catalytic performance of CuO/kaolin NC-1 is considerably better than that of other nanocomposites. Thus, CuO/kaolin NC-1 was the best catalyst for further experiments.

**3.5. Effect of Catalyst Amount.** To study the effect of the amount of CuO/kaolin NC-1 on the reduction of 4-NP, different masses of composite (2.5, 5, 7.5, and 10 mg) were investigated in the reaction mixture while other experimental conditions remained unchanged. The corresponding time-dependent UV−vis absorption spectra changes are displayed in Figures 10A and S5A−C. Figure 10B displayed the effect of catalyst dose on the reduction of 4-NP by $NaBH_4$ in the presence of CuO/kaolin NC-1 catalyst, and Figure 10C shows the corresponding plots of $\ln(A_t/A_0)$ versus reaction time on which the $k_{app}$ values were calculated from the slope of $\ln(A/A_0)$ versus reaction time plot (Table 2). The time required for the catalytic reduction of 4-NP to 4-AP by $NaBH_4$ decreased as the amount of CuO/kaolin NC-1 increased, from 2.5 (12 min, Figure S5A) to 5 mg (6 min, Figure 10A). The results showed that the catalytic degradation rate of 4-NP was increased by increasing the CuO/kaolin NC-1 dose. The primary reason for this behavior is that as the amount of CuO/kaolin NC-1 increased, the active sites of the catalyst also increased, allowing reactants to be adsorbed on their surfaces. This is in agreement with other reports.[20] Continuously increasing the catalyst to 7.5 mg, the time required for the catalytic reduction of 4-NP remained the same (6 min, Figure S5B). The reaction rate slightly decreased as compared to the 5 mg catalyst amount (Table 2), indicating that CuO/kaolin NC-1 has a good catalytic efficiency. However, 10 mg of the CuO/kaolin NC-1 catalyst required much time to obtain the complete conversion of 4-NP (7 min, Figure S5C). This trend may be related to the excellent dispersion of the catalyst at a low loading amount in the aqueous solution.[57] As shown in Figures 10D and S5D, 99.55 and 99.04% of 4-NP reduction over CuO/kaolin NC-1 was obtained using 5 and 7.5 mg of catalyst at a reaction time of 3 min, while only 90.2% was obtained in 10 mg of catalyst at the same reaction time. These results suggest that 5 mg of CuO/kaolin NC-1 is the optimal amount of catalyst for the reaction.

**Table 2. Apparent Rate Constants, Percent Reduction, and Time Taken to Complete the Reaction for the Catalytic Reduction of 20 mg $L^{-1}$ 4-NP by $NaBH_4$ at Different CuO/Kaolin NC-1 Catalyst Dose**

| catalyst mass (mg) | 4-NP solution (mg $L^{-1}$, 50 mL) | rate constant ($min^{-1}$) | time (min) | %R |
|---|---|---|---|---|
| 5 | 20 | 1.21 | 6 | 99.55 |
| 2.5 | | 0.62 | 12 | 99.52 |
| 7.5 | | 0.99 | 6 | 99.04 |
| 10 | | 0.84 | 7 | 99.20 |

**3.6. Effect of 4-NP Initial Concentrations.** The influence of 4-NP initial concentration on the catalytic activity of CuO/kaolin NC-1 for the reduction of 4-NP by $NaBH_4$ was studied by varying its concentration from 10 to 30 mg $L^{-1}$ while keeping other reaction conditions unchanged. The effect of 4-NP initial concentration on the reduction of 4-NP by $NaBH_4$ catalyzed by CuO/kaolin NC-1 and the corresponding plots of $\ln(A_t/A_0)$ against reaction time are shown in Figure 11B,C, respectively. The $k_{app}$ values were obtained from the slope of the plot of $\ln(A/A_0)$ versus reaction time (Table 3). At 10 mg $L^{-1}$ of 4-NP used, a slightly slower reduction rate was observed compared to the 15 mg $L^{-1}$ of 4-NP reduction rate. However, the complete reduction was achieved in just 6 min (Figure S6A,B), which could be attributed to the lower collision probability between 4-NP and the catalyst particles.[54,58] Continuously increasing the 4-NP concentration to 20 mg $L^{-1}$, the reaction rate decreased only slightly, and the reduction completion was achieved within 6 min (Figure 11A), demonstrating the good catalytic efficiency of CuO/kaolin NC-1. The rate of reaction significantly dropped upon raising the 4-NP initial concentration to 30 mg $L^{-1}$, and the complete reduction of the reaction was reached virtually in 8 min (Figure S6C). This result demonstrated that the CuO NPs on the kaolin surface have insufficient active sites for the relatively higher amount of 4-NP. As shown in Figures 11D and S6D, the catalytic performance of CuO/kaolin NC-1 is greatly better in concentrations not higher than 20 mg $L^{-1}$ of 4-NP. These results suggest that 20 mg $L^{-1}$ of 4-NP is the optimal amount of 4-NP concentration for the reduction of 4-NP by $NaBH_4$ over the CuO/kaolin NC-1 reaction.

**3.7. Effect of $NaBH_4$ Amount.** To reduce 4-NP, $NaBH_4$ is required. Higher quantities, however, are poisonous because of the presence of boron in addition to the harsh reaction. Although many studies have used higher concentrations of $NaBH_4$ than 4-NP to achieve a higher reaction rate and an ideal fit in the pseudo-first-order reaction plot, it is crucial to take into account the 2.4 $\mu g$ $mL^{-1}$ boron toxicity limit set by the World Health Organization (WHO) and the Environmental Protection Agency (EPA).[4] Naturally, if the concentration of $NaBH_4$ is smaller, the catalytic reduction reaction


https://doi.org/10.1021/acsomega.4c04029
ACS Omega 2024, 9, 48014−48031

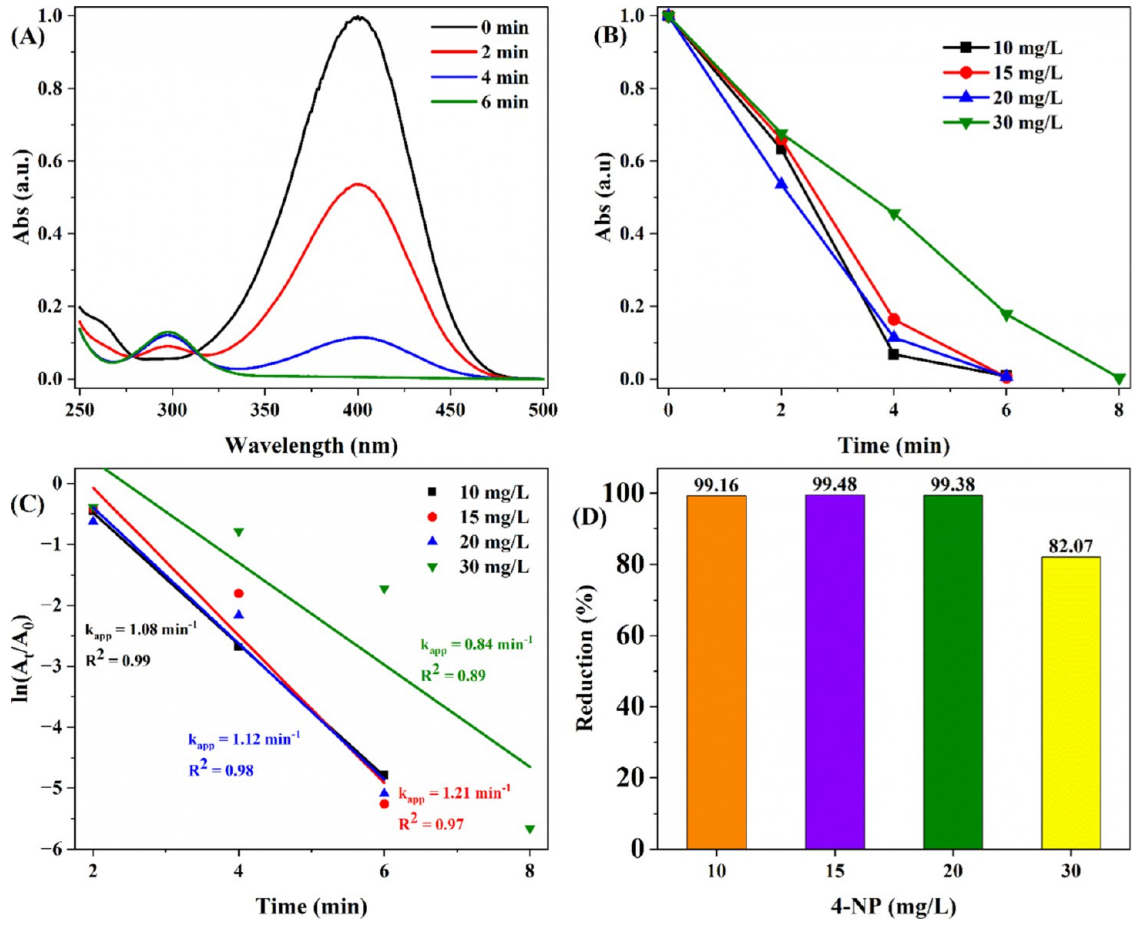


**Figure 11.** (A) UV−vis time-dependent absorption spectra changes of 4-NP using 20 mg $L^{-1}$ of 4-NP. (B) The plots of absorbance against reaction time for the reduction of 4-NP using various concentrations of 4-NP. (C) The corresponding plots of $\ln(A_t/A_0)$ against reaction time. (D) Reduction efficiency of 4-NP over CuO/kaolin NC-1 using various 4-NP concentrations within 6 min reaction time. Reaction conditions: 0.132 mmol $NaBH_4$; 5 mg CuO/kaolin NC-1; 22 °C.

**Table 3. Apparent Rate Constants, Time Taken, and Reduction Efficiencies of 4-NP Reduction by $NaBH_4$ Catalyzed by CuO/Kaolin NC-1 at Different Concentrations of 4-NP**

| catalyst mass | [4-NP] (mg $L^{-1}$, 50 mL) | $k_{app}$ ($min^{-1}$) | time (min) | %R |
|---|---|---|---|---|
| 5 | 10 | 1.08186 | 6 | 99.16376 |
| | 15 | 1.21105 | 6 | 99.47966 |
| | 20 | 1.11681 | 6 | 99.38473 |
| | 30 | 0.71211 | 8 | 82.06967 |

can take a longer time to complete, but avoiding boron purification is crucial. Therefore, optimizing the sufficient amount of $NaBH_4$ in the reduction of 4-NP over a given catalyst instead of adding excess concentration is very important. In this study, a series of reductions were carried out by varying the mass of $NaBH_4$ added (5, 10, and 15 mg) in the reaction system while keeping the concentration of 4-NP and catalyst quantity constant. The corresponding time-dependent UV−vis absorption spectra plots are shown in Figures 12A and S7A,B. The effect of $NaBH_4$ amount on 4-NP reduction in the presence of CuO/kaolin NC-1 is shown in Figure 12B. At a constant 4-NP concentration and catalyst amount, the increase in $NaBH_4$ amount significantly increased the reaction rate. However, the presence of a sufficient reducing agent, which was thought to be constant and had no effect on the reaction rate, diminished the effect of the $NaBH_4$ amount when it was increased to 15 mg. The corresponding plots of $\ln(A_t/A_0)$ against reaction time are displayed in Figure 12C. As shown in Figures 12D and S7C, 99.55% of 4-NP reduction over CuO/kaolin NC-1 was obtained using 10 mg of $NaBH_4$ at a reaction time of 3 min, while 99.58% was obtained in 15 mg of $NaBH_4$. These results suggest that 10 mg of $NaBH_4$ is the optimal amount for the reduction of 4-NP. Table 4 compares and reports the reaction rate constants for CuO/kaolin NC-1 under optimized conditions and various other catalysts for 4-NP reduction by $NaBH_4$. According to the results, the as-synthesized nanocomposite in this study may be one of the best catalysts for 4-NP reduction in aqueous environments.

**3.8. Effect of Temperature and Reaction Thermodynamics.** For evaluating the thermodynamics of the catalyzed reaction, the reduction of 4-NP was investigated at four different temperatures in the room temperature range of 22 to 42 °C, and the corresponding UV−vis absorption changes are shown in Figures 13A and S8A−C. The influences of the reaction temperatures on 4-NP reduction by $NaBH_4$ over CuO/kaolin NC-1 are shown in Figure 13B. The relations between $\ln(A_t/A_0)$ and reaction time at various temperatures are plotted in Figure 13C, which was used to calculate the associated $k_{app}$ values from the slope of the curve and are listed in Table 5. The $k_{app}$ gradually increases with temperatures from


https://doi.org/10.1021/acsomega.4c04029
ACS Omega 2024, 9, 48014−48031

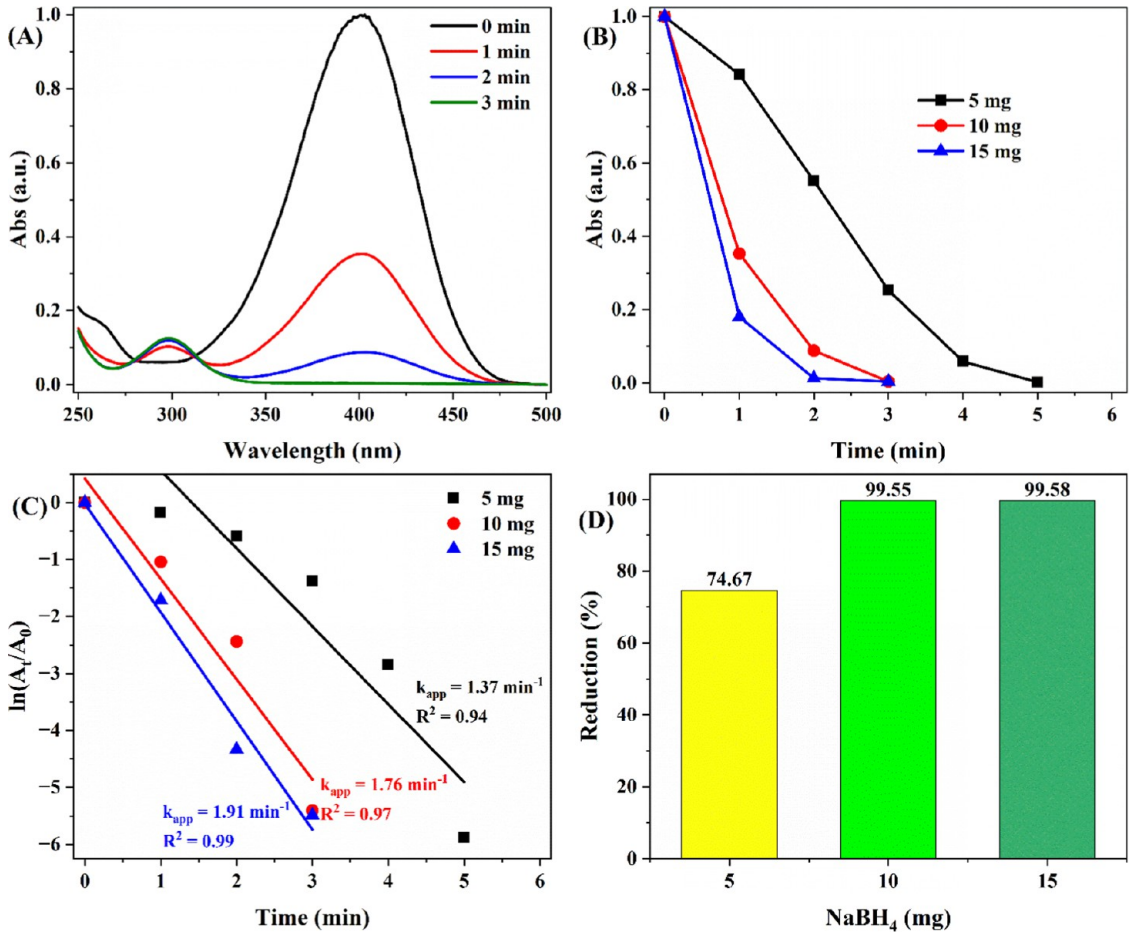


**Figure 12.** (A) UV−vis time-dependent absorption spectra changes of 4-NP using 10 mg of $NaBH_4$. (B) The plots of absorbance against reaction time for the reduction of 4-NP using various $NaBH_4$ amounts. (C) The corresponding plots of $\ln(A_t/A_0)$ against reaction time. (D) Reduction efficiency of 4-NP over CuO/kaolin NC-1 using various $NaBH_4$ amounts within 3 min reaction time. Reaction conditions: 20 mg $L^{-1}$, 50 mL of 4-NP; 5 mg CuO/kaolin NC-1; 22 °C.

**Table 4. Comparison of the Reduction Efficiency of 4-NP by $NaBH_4$ over CuO/Kaolin NC-1 and CuO NPs with Related Catalysts Reported in the Literature**

| catalyst | amount of 4-NP (mmol) | amount of $NaBH_4$ (mmol) | catalyst amount (mg) | reaction time (min) | $k_{app}$ ($min^{-1}$) | refs |
|---|---|---|---|---|---|---|
| CuO/kaolinNC-1 | 0.007 | 0.264 | 5 | 6 | 1.76 | this work |
| CuO NPs | 0.007 | 0.264 | 5 | 10 | 0.09 | this work |
| Au/ZnO nanoflowers | 0.0005 | 0.02 | 20 | 11 | 0.236 | 9 |
| CuBDC·DMF | 0.1 | 2.25 | 50 | 5 | 0.906 | 59 |
| CuO/g-$C_3N_4$ | 0.0001 | 0.01 | 1 | 7 | 0.784 | 60 |
| Au-m-$Co_3O_4$ | 0.0005 | 0.04 | 2 | 5 | 0.83 | 61 |
| Co-MoN-MgO/C | 0.006 | 0.185 | 5 | 1.5 | 0.41 | 62 |
| $Pd_1$-$(Ni_xO_y)_{1/x}$@HPSNs | 0.05 | 2.5 | 3 | 6 | 0.99 | 54 |
| $Co_3O_4$/HNTs | 0.000348 | 0.139 | 0.1 | 11 | 0.265 | 20 |
| $Au_1$-$(Cu_xO_y)_{0.8/x}$ in HPSNs | 0.025 | 1.5 | 5 | 5.5 | 0.96 | 58 |
| Kaolin@CS-Pectine/Pd | 0.0075 | 0.00025 | | 6 | | 23 |
| Ag/Hal/PVA | 0.006 | 2.4 | | 14 | 0.297 | 63 |
| Ag@TzTFB-COF | 0.002 | | 2 | 2.33 | 1.11 | 64 |

1.30 $min^{-1}$ at 22 °C to 1.84 $min^{-1}$ at 28 °C. Further increasing the temperature to 35 °C, the $k_{app}$ rapidly increased to 2.81 $min^{-1}$, which indicated there was a great chance of collisions and faster molecular motions at higher temperatures, while this value decreased to 2.24 $min^{-1}$ at 42 °C, which could be related to the extent of 4-NP and hydrogen adsorption decreased at higher temperatures.[65] More than 99% of 4-NP reduction was obtained in just 2 min at 36 °C (Figure 13D). In addition, Figure S8D also shows the percentage reduction of 4-NP over the reduction procedure using different reaction temperatures.

Based on the reaction rates at different temperatures, the apparent activation energy ($E_a$) for 4-NP reduction by $NaBH_4$ over CuO/kaolin NC-1 could be determined from the plot of $\ln k_{app}$ against $1000/T$ (Figure 14A) according to the Arrhenius equation (eq 5)


https://doi.org/10.1021/acsomega.4c04029
ACS Omega 2024, 9, 48014−48031

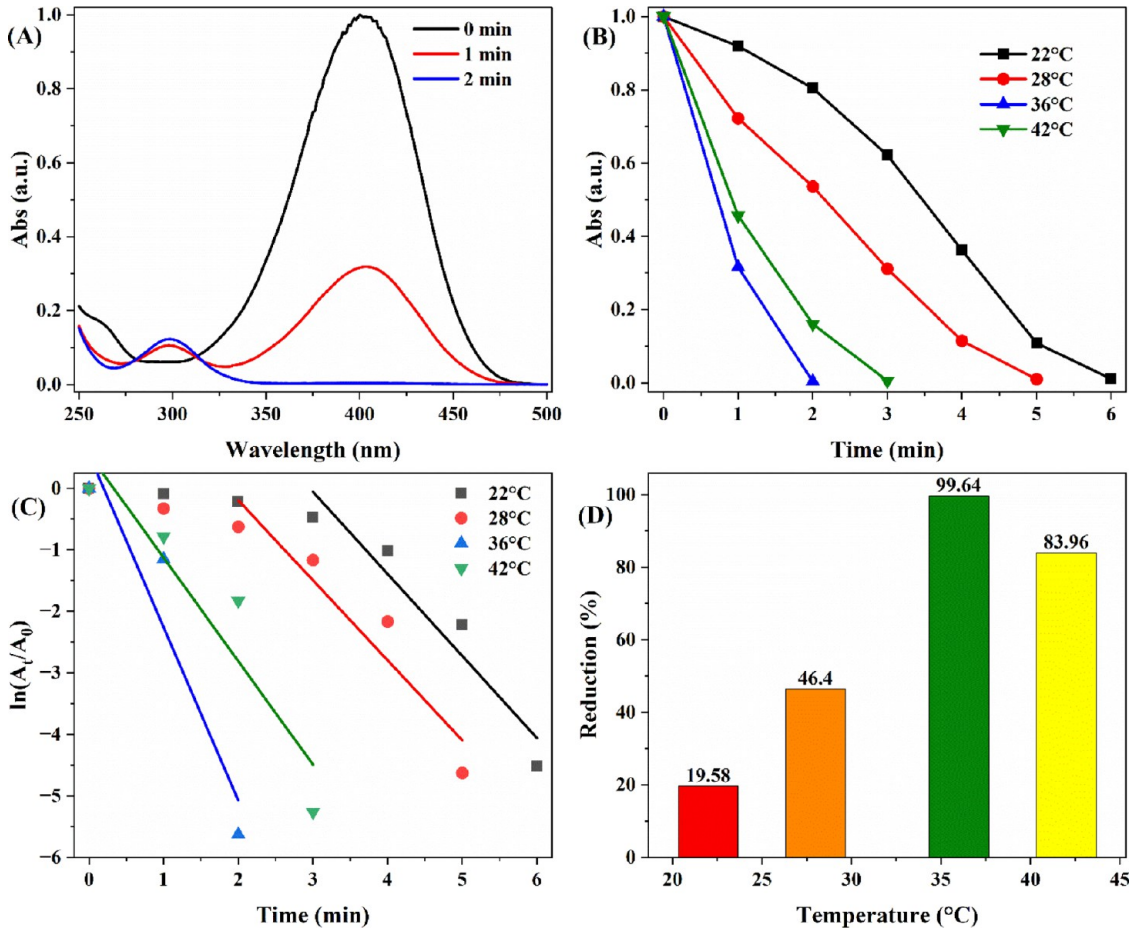


**Figure 13.** (A) UV−vis time-dependent absorption spectra changes of 4-NP reduction at 36 °C. (B) The plots of absorbance against reaction time for the reduction 4-NP at different temperatures. (C) The corresponding plots of $\ln(A_t/A_0)$ against reaction time. (D) Reduction of 4-NP over various temperatures within 2 min reaction time. Reaction conditions: 20 mg $L^{-1}$, 50 mL of 4-NP; 0.132 mmol $NaBH_4$; 5 mg CuO/kaolin NC-1.

**Table 5. Summary of Apparent Rate Constants, Activation Energy, and Thermodynamic Parameters for Reduction of 4-NP Catalyzed by CuO/Kaolin NC at Different Reaction Temperatures**

| temperature (K) | $k_{app}$ ($min^{-1}$) | $E_a$ (kJ $mol^{-1}$) | $\Delta H^{\neq}$ (kJ $mol^{-1}$) | $\Delta S^{\neq}$ (J $mol^{-1}$ $K^{-1}$) | $\Delta G^{\neq}$ (kJ $mol^{-1}$) |
|---|---|---|---|---|---|
| 295 | 1.30 | 41.7 | 38.055 | −113.52 | 71.543 |
| 301 | 1.84 | | | | 72.224 |
| 309 | 2.81 | | | | 73.132 |
| 315 | 2.24 | | | | 73.813 |

$$\ln k_{app} = \ln A - \frac{E_a}{RT} \quad (5)$$

where $R$ is the universal gas constant, $T$ is the absolute temperature (in kelvin), and $\ln A$ is the intercept of the line. The $E_a$ value is found to be 41.7 kJ $mol^{-1}$ and which is in close agreement with previously published nanocatalysts, including Ag@TzTFB-COF (36.64 kJ $mol^{-1}$),[64] Co-MoN-MgO/C (35.68 kJ $mol^{-1}$),[62] Pd-$Ni_xO_y$@HPSNs (47.1 kJ $mol^{-1}$),[54] $Au_1$-$(Cu_xO_y)_{0.8/x}$ in HPSNs (46.56 kJ $mol^{-1}$),[58] and Au/ZnO nanoflowers (32.46 kJ $mol^{-1}$).[9] The result thus proved that the 4-NP reduction reaction occurs on the catalyst surface.

Furthermore, the thermodynamic parameters like the enthalpy of activation ($\Delta H^{\#}$) and entropy of activation ($\Delta S^{\#}$) were calculated from the plot of $\ln(k_{app}/T)$ against $1000/T$ (Figure 14B) using the Eyring equation (eq 6)

$$\ln\left(\frac{k_{app}}{T}\right) = \ln\left(\frac{k_B}{h}\right) + \frac{\Delta S^{\#}}{R} - \frac{\Delta H^{\#}}{RT} \quad (6)$$

where $k_B$ is the Boltzmann constant ($1.38 \times 10^{-23}$ J $K^{-1}$) and $h$ is the Planck's constant ($6.626 \times 10^{-34}$ J s). The calculated values of $\Delta H^{\#}$and $\Delta S^{\#}$ are 38.055 kJ $mol^{-1}$ and −113.52 J $mol^{-1}$ $K^{-1}$, respectively. The positive $\Delta H^{\#}$ values indicate that the reaction between 4-NP and CuO NPs to create an activated complex was endothermic. Additionally, the negative value of $\Delta S^{\#}$ suggests that the molecules of 4-NP and CuO NPs formed an activated complex.[66] Moreover, the Gibbs free energy ($\Delta G^{\#}$) could be calculated using eq 7; the results are displayed in Table 5.

$$\Delta G^{\#} = \Delta H^{\#} - T\Delta S^{\#} \quad (7)$$

The value of $\Delta G^{\#}$ was positive in the adsorption of 4-NP on the surface of CuO NPs, indicating that the reaction was nonspontaneous and required energy to transform reactants


https://doi.org/10.1021/acsomega.4c04029
ACS Omega 2024, 9, 48014−48031

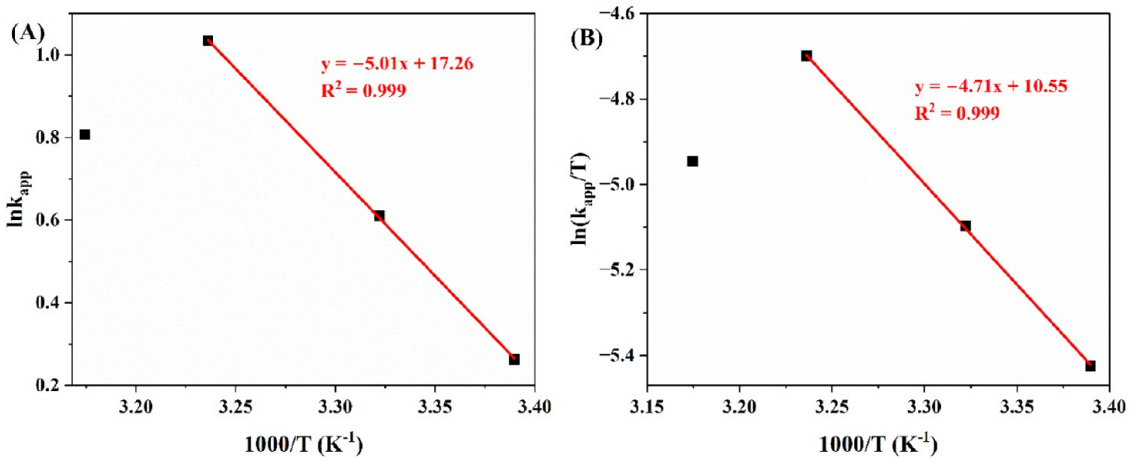


**Figure 14.** (A) Arrhenius plot of ln $k_{app}$ against 1000/$T$ for the reduction of 4-NP at different temperatures in the presence of CuO/kaolin NC-1. (B) The plot of ln($k_{app}$/$T$) against 1000/$T$ for 4-NP reduction at different temperatures over CuO/kaolin NC-1. Reaction conditions: 20 mg $L^{-1}$, 50 mL of 4-NP; 0.132 mmol $NaBH_4$; 5 mg CuO/kaolin NC-1.

**Scheme 2. Schematic Diagrams of the Proposed Mechanism for the Catalytic Reduction Reaction of 4-NP by $NaBH_4$ over the CuO/Kaolin NC**

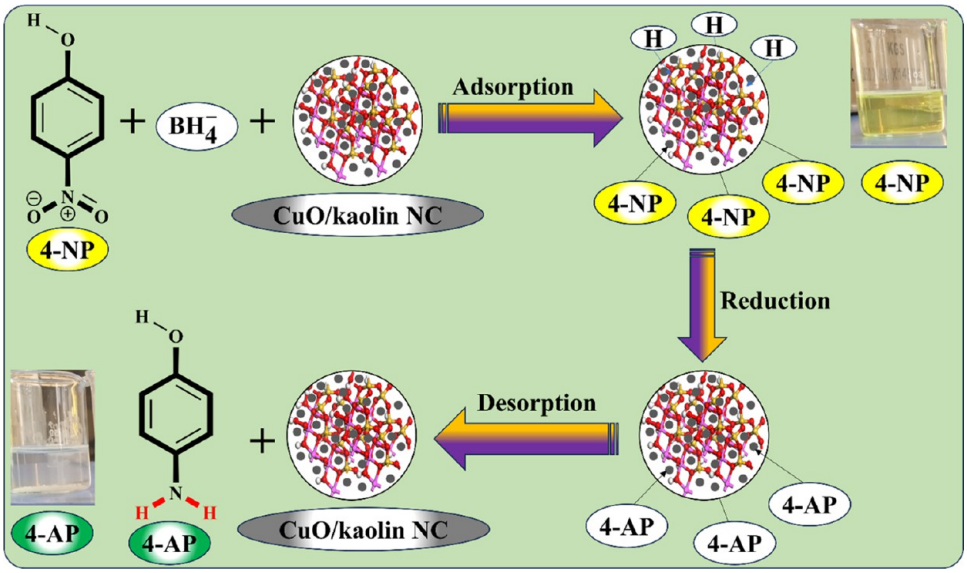


into products. In addition, the increased Gibbs free energy from 71.543 kJ $mol^{-1}$ at 295 K to 73.813 kJ $mol^{-1}$ at 315 K suggests that the reaction requires energy. Thus, the results confirmed that the temperature increase provided energy to the reaction system.

**3.9. Proposed Catalytic Reduction Mechanism of 4-NP.** The catalytic reduction mechanism of 4-NP to 4-AP by excess $NaBH_4$ is typically explained by the Langmuir−Hinshelwood (L−H) kinetic model.[64] This mechanism states that the catalytic reduction process is facilitated by the metallic oxide nanostructure's surface.[67,68] The $BH_4^-$ ions attach to the surface of CuO NPs by adsorption, transferring hydrogen species to the surface of NPs. at the same time, 4-NP adsorbs on the surface and is reduced to 4-AP by the action of hydrogen species.[14] In addition, the reaction medium's aqueous phase supplied the $H^+$ ions required to finish the reduction process.[69] The 4-AP products are finally desorbed from the CuO NPs' surface, allowing the subsequent catalytic cycle to begin. Scheme 2 depicts the suggested method for the catalytic reduction reaction of 4-NP by $NaBH_4$ over CuO NPs loaded into kaolin sheets.

A heterogeneous catalytic reduction reaction occurs when nitrophenols are reduced catalytically using CuO/kaolin NC. Regarding the L−H mechanism, the reaction starts when both the substrate molecules, nitrophenol and $BH_4^-$, get adsorbed on the catalyst's surface.[68] Two methods can be used to study a reaction mechanism for the reduction of 4-NP: (1) calculating $k_{app}$ values with varying 4-NP concentrations and (2) calculating $k_{app}$ values with varying $NaBH_4$ concentrations. The $k_{app}$ value in the L−H mechanism rises with $NaBH_4$ concentration while falling with 4-NP concentration. With regard to 4-NP concentration, we know that the reduction reaction of 4-NP catalyzed by CuO/kaolin NC is a PFO reaction. The surface area of the materials determines the $k_{app}$ values of the 4-NP catalytic reduction reaction. Figure S9A shows the plot of the $k_{app}$ values against the concentration of 4-NP in CuO/kaolin NC at room temperature at a fixed concentration of $NaBH_4$ of 0.32 mmol (5 mg). As the initial concentration of 4-NP increased, the $k_{app}$ values declined.


https://doi.org/10.1021/acsomega.4c04029
ACS Omega 2024, 9, 48014−48031

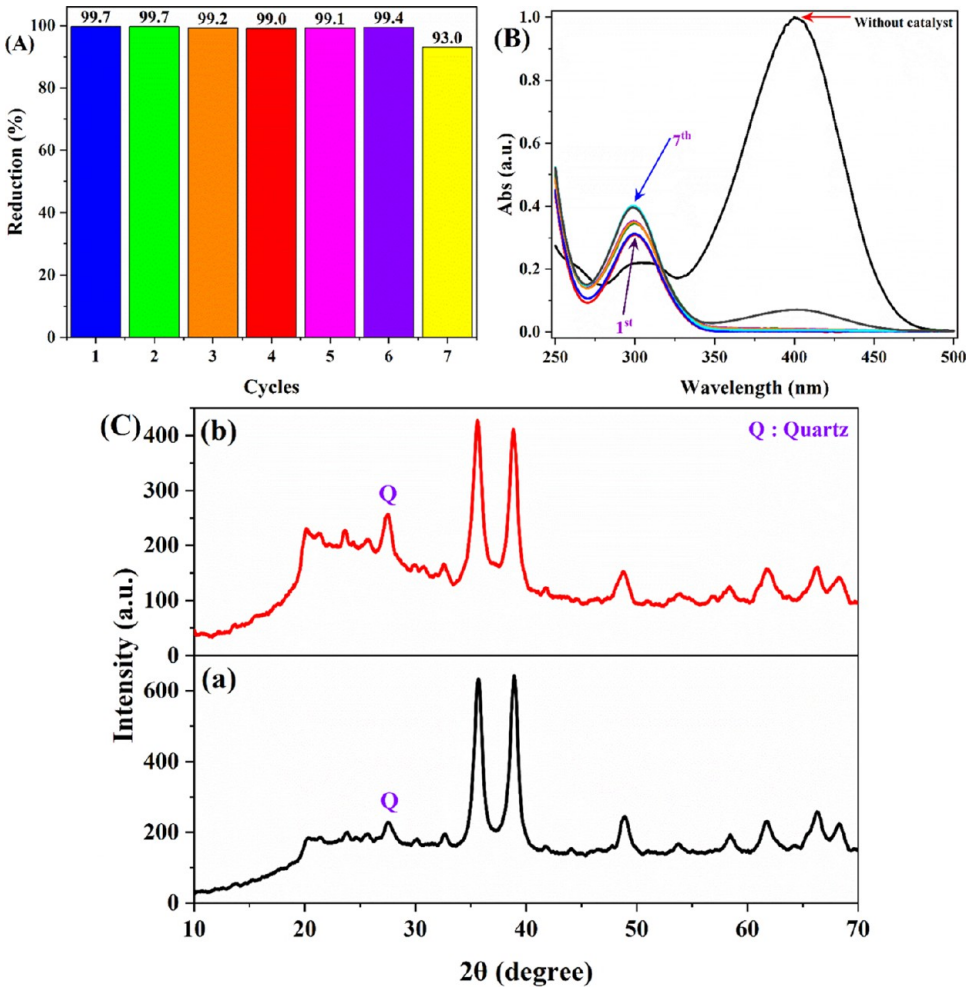


**Figure 15.** (A) Reductions at 5 min of each run. (B) The UV−vis time-dependent absorption spectra of 4-NP reduction by CuO/kaolin NC-1 for 7 cycles. (C) The XRD patterns of CuO/kaolin NC-1 before used (a) and after 7th cycles used (b) toward the reduction of 4-NP.

Similarly, Figure S9B shows the plot of $k_{app}$ values versus the concentration of $NaBH_4$ in the presence of CuO/kaolin NC at room temperature, with a fixed concentration of 4-NP of 20 mg $L^{-1}$. As clearly shown in the figure, with the increase in $NaBH_4$, the $k_{app}$ values increased. The reduction of 4-NP therefore proceeds following the L−H mechanism, as evidenced by the nonlinear change of the $k_{app}$ values with regard to the initial concentration of 4-NP and $NaBH_4$ amount. With an increase in 4-NP concentration, more molecules are adsorbed at the CuO/kaolin NC surface; because of this, the surface becomes saturated with 4-NP molecules. As a result, the concentration of $BH_4^-$ ions approaching the CuO/kaolin NC surface decreases, which in turn slows down the rate at which hydrogen is transferred from the $BH_4^-$ ion to the 4-NP molecule. This demonstrates that the L-H mechanism explains the 4-nitrophenol reduction reaction that CuO/kaolin NC catalyzes.

**3.10. Reusability of CuO/Kaolin Nanocomposite.** The most significant criterion in evaluating the potential of the catalyst materials for widespread practical application is their reusability. Thus, the reusability of CuO/kaolin NC-1 was examined in seven consecutive cycles of the 4-NP catalytic reduction reaction procedure. As shown in Figure 15A, the catalyst maintained >99.7% of its 4-NP reduction capacity during six successive reaction cycles. After seven reaction cycles, the results show 93% retention of catalytic performance, indicating the stability of the catalyst. In the corresponding UV−vis spectra (Figure 15B), the peak appearance of 4-AP at 300 nm and the disappearance of the peak of 4-NP anions at 400 nm during the seven cycles are visible indicating that repeated use does not affect the material's catalytic activity. The decrease in catalytic efficiency after the six cycles might be due to the aggregation and decrease of active sites of the catalyst because of mass loss during filtration.[65] It is supported by the XRD pattern (Figure 15C) of the used catalyst, which reveals that the crystallite size is increased to 21.6 nm for the used CuO/kaolin NC-1 catalyst. As shown in Figure 15C, the diffraction planes of CuO NPs after use (Figure 15C(b)) are comparatively decreased in intensities than before use (Figure 15C(a)). This is supported by the increased intensities of the calcined kaolin amorphous portion ($2\theta$ = 15−35°) and the quartz peak (Figure 15C(b)). Overall, the outcome showed that the high reusability of the CuO/kaolin NC-1 may be attributed to the effective stability of CuO NPs and better adhesion to the kaolin surface, which prevents catalyst loss and preserves the active sites for catalysis. Hence, the high stability and reusability of the CuO/kaolin NC-1 ensure its great potential use for long-term catalytic application in removing hazardous pollutants in wastewater effluents.


https://doi.org/10.1021/acsomega.4c04029
ACS Omega 2024, 9, 48014−48031

## 4. CONCLUSIONS

Locally available and inexpensive kaolin-supported CuO nanoparticles were successfully prepared. CuO/kaolin NC-1 was characterized by XRD, FT-IR, UV−vis, SEM-EDX, TEM, HAADF-STEM, and $N_2$ adsorption/desorption analysis. Under mild conditions, the CuO/kaolin NC-1 was an efficient catalyst for reducing 4-NP into 4-AP by $NaBH_4$ in aqueous medium. The CuO/kaolin catalyst (5 mg) degraded >99% of 4-NP aqueous solution (20 mg $L^{-1}$, 50 mL) within 6 min in the presence of $NaBH_4$ under ambient reaction conditions, with a rate constant of 1.76 $min^{-1}$. The CuO/kaolin NC-1 increased the catalytic reduction rate of 4-NP by factors of 4.44 compared with CuO NPs, demonstrating the critical role of the kaolin substrate. Furthermore, the CuO/kaolin NC-1 catalyst maintained 93% of its activity after recycling for seven cycles, with its structural integrity maintained as confirmed by XRD analysis, demonstrating its good durability. The robust kaolin support contributed to the catalyst's stability, showing no significant loss in efficiency or activity over multiple cycles. Moreover, the thermodynamic parameters determined by the Arrhenius and Eyring equations showed values of $E_a$ (41.7 kJ $mol^{-1}$), $\Delta H^{\#}$ (38.055 kJ $mol^{-1}$), $\Delta S^{\#}$ (−113.52 J $mol^{-1}$ $K^{-1}$), and $\Delta G^{\#}$ (71.54−73.81 kJ $mol^{-1}$) across a temperature range of 295−315 K. The findings of this study have practical applications in developing highly effective metal oxide nanocatalysts that employ kaolin as a substrate for nitrophenol reduction, paving the way for further applications in environmental remediation and industrial catalysis.

## ■ ASSOCIATED CONTENT

### Supporting Information

The Supporting Information is available free of charge at https://pubs.acs.org/doi/10.1021/acsomega.4c04029.

2D structure of kaolin (Figure S1); FE-SEM images of CuO/kaolin NC-1 (Figure S2); the UV−vis absorption spectra of 4-NP with and without $NaBH_4$ in the presence of catalyst and percentage removal (Figure S3); time dependent UV−vis absorption spectra of 4-NP reduction catalyzed by various nanocomposites (Figure S4); UV−vis absorption spectra of 4-NP reduction by $NaBH_4$ using various catalyst dose (Figure S5); time dependent UV−vis absorption spectra of 4-NP reduction catalyzed by CuO/kaolin NC-1 using various 4-NP initial concentrations (Figure S6); UV−vis absorption spectra of 4-NP reduction over CuO/kaolin NC-1 using various $NaBH^4$ amounts (Figure S7); UV−vis absorption spectra changes of 4-NP reduction over CuO/kaolin NC-1 with different reaction temperatures (Figure S8); and the plot of $k_{app}$ versus 4-NP concentration and $NaBH_4$ amount (PDF)

## ■ AUTHOR INFORMATION


### Corresponding Authors

**Belete Asefa Aragaw** − *Chemistry Department, College of Science, Bahir Dar University, 79 Bahir Dar, Ethiopia;* orcid.org/0000-0003-4801-7197; Email: beliyeeed@gmail.com

**Minaleshewa Atlabachew** − *Chemistry Department, College of Science, Bahir Dar University, 79 Bahir Dar, Ethiopia;* orcid.org/0000-0003-3261-8326; Email: atminale2004@yahoo.com

### Author

**Zinabu Gashaw Asmare** − *Chemistry Department, College of Science, Bahir Dar University, 79 Bahir Dar, Ethiopia; Chemistry Department, College of Natural and Computational Sciences, Debre Tabor University, 272 Debre Tabor, Ethiopia;* orcid.org/0000-0002-8945-6172

Complete contact information is available at: https://pubs.acs.org/10.1021/acsomega.4c04029


### Notes

The authors declare no competing financial interest.

## ■ ACKNOWLEDGMENTS

By way of sponsoring his doctoral studies, Z.G.A. thanks Debre Tabor University. The Bahir Dar University College of Science provided the laboratory space needed for this investigation, for which the authors are grateful.

## ■ REFERENCES


(1) Aziz, K. H. H.; Mustafa, F. S.; Omer, K. M.; Hama, S.; Hamarawf, R. F.; Rahman, K. O. Heavy metal pollution in the aquatic environment: efficient and low-cost removal approaches to eliminate their toxicity: a review. *RSC Adv.* **2023**, *13* (26), 17595−17610.

(2) Filiz, B. C. The role of catalyst support on activity of copper oxide nanoparticles for reduction of 4-nitrophenol. *Adv. Powder Technol.* **2020**, *31* (9), 3845−3859.

(3) Ding, M.; Peng, B.; Zhou, J.-F.; Chen, H.; Zhu, Y.-S.; Yuan, E.-H.; Albela, B.; Bonneviot, L.; Wu, P.; Zhang, K. Molecular Manipulation of the Microenvironment of Au Active Sites on Mesoporous Silica for the Enhanced Catalytic Reduction of 4-Nitrophenol. *Catal. Sci. Technol.* **2023**, *13* (7), 2001−2009.

(4) Mejía, Y. R.; Bogireddy, N. K. R. Reduction of 4-Nitrophenol Using Green-Fabricated Metal Nanoparticles. *RSC Adv.* **2022**, *12*, 18661−18675.

(5) Toropov, A. A.; Toropova, A. P.; Roncaglioni, A.; Benfenati, E. In Silico Prediction of The Mutagenicity of Nitroaromatic Compounds Using Correlation Weights of Fragments of Local Symmetry. *Mutat. Res., Genet. Toxicol. Environ. Mutagen.* **2023**, *891*, No. 503684.

(6) Deka, P.; Borah, B. J.; Saikia, H.; Bharali, P. Cu-Based Nanoparticles as Emerging Environmental Catalysts. *Chem. Rec.* **2019**, *19* (2−3), 462−473.

(7) Wanjari, V. P.; Duttagupta, S. P.; Singh, S. P. Dual Linear Range Laser-Induced Graphene-Based Sensor for 4-Nitrophenol Detection in Water. *ACS Appl. Nano Mater.* **2023**, *6* (13), 11351−11360.

(8) Akhtar, T.; Hill, A. J.; Bhat, A.; Schwank, J. W.; Nasir, H.; Bukhari, S. A. B.; Sitara, E. Fabrication of Ruthenium Doped Ag@$TiO_2$ Core-Shell Nanophotocatalyst for The Efficient Reduction of Nitrophenols. *Appl. Surf. Sci.* **2023**, *630*, No. 157491.

(9) Biswas, R.; Banerjee, B.; Saha, M.; Ahmed, I.; Mete, S.; Patil, R. A.; Ma, Y.-R.; Haldar, K. K. Green Approach for the Fabrication of Au/ZnO Nanoflowers: A Catalytic Aspect. *J. Phys. Chem. C* **2021**, *125* (12), 6619−6631.

(10) Bagheri, M.; Masoomi, M. Y.; Forneli, A.; García, H. A Quasi-Metal−Organic Framework Based on Cobalt for Improved Catalytic Conversion of Aquatic Pollutant 4-Nitrophenol. *J. Phys. Chem. C* **2022**, *126* (1), 683−692.

(11) Houcini, H.; Laghrib, F.; Bakasse, M.; Lahrich, S.; El Mhammedi, M. A. Catalytic Activity of Gold for The Electrochemical Reduction of P-Nitrophenol: Analytical Application. *Int. J. Environ. Anal. Chem.* **2020**, *100* (14), 1566−1577.

(12) Patar, S.; Konwer, S.; Chetia, T.; Bhuyan, B. K.; Borthakur, L. J. Photocatalytic Nanojunction of Cobalt Ferrite Anchored Sulfonated Graphene for Reduction of Nitrophenols. *ACS Appl. Nano Mater.* **2023**, *6* (8), 6567−6580.

(13) Raza, W. Catalytic Reduction of 4-Nitrophenol to 4-Aminphenol in Water Using Metal Nanoparticles. In *Sustainable*

*Materials and Green Processing for Energy Conversion*; Cheong, K. Y.; Apblett, A., Eds.; Elsevier, 2022; Chapter 7, pp 237−261.
(14) Aditya, T.; Pal, A.; Pal, T. Nitroarene reduction: a trusted model reaction to test nanoparticle catalysts. *Chem. Commun.* **2015**, *51* (46), 9410−9431.
(15) Audemar, M.; Vallcorba, O.; Peral, I.; Thomann, J.-S.; Przekora, A.; Pawlat, J.; Canal, C.; Ginalska, G.; Kwiatkowski, M.; Duday, D.; Hermans, S. Catalytic Enrichment of Plasma with Hydroxyl Radicals in The Aqueous Phase at Room Temperature. *Catal. Sci. Technol.* **2021**, *11* (4), 1430−1442.
(16) Ramirez, L. A.; Dennehy, M.; Alvarez, M. Metal Oxide-Biochar Supported Recyclable Catalysts: A Feasible Solution for The Reduction of 4-Nitrophenol in Water. *Catal. Commun.* **2023**, *181*, No. 106723.
(17) Amirjan, M.; Nemati, F.; Elahimehr, Z.; Rangraz, Y. Copper Oxides Supported Sulfur-Doped Porous Carbon Material as a Remarkable Catalyst for Reduction of Aromatic Nitro Compounds. *Sci. Rep.* **2024**, *14* (1), No. 5491.
(18) Jacob, B.; Mohan, M.; Dhanyaprabha, K. C.; Thomas, H. Facile One Pot Synthesis of Nitrogen-Doped Reduced Graphene Oxide Supported $Co_3O_4$ Nanoparticles as Bifunctional Catalysts for the Reduction of 4-Nitrophenol and $NaBH_4$ Hydrolysis. *Int. J. Hydrogen Energy* **2023**, *48* (25), 9285−9305.
(19) Da'na, E.; Taha, A.; El-Aassar, M. R. Catalytic Reduction of p-Nitrophenol on MnO2/Zeolite −13X Prepared with Lawsonia inermis Extract as a Stabilizing and Capping Agent. *Nanomaterials* **2023**, *13* (4), No. 785.
(20) Zhang, M.; Su, X.; Ma, L.; Khan, A.; Wang, L.; Wang, J.; Maloletnev, A.; Yang, C. Promotion Effects of Halloysite Nanotubes on Catalytic Activity of $Co_3O_4$ Nanoparticles toward Reduction of 4-Nitrophenol and Organic Dyes. *J. Hazard. Mater.* **2021**, *403*, No. 123870.
(21) Wassel, A. R.; El-Naggar, M. E.; Shoueir, K. Recent Advances in Polymer/Metal/Metal Oxide Hybrid Nanostructures for Catalytic Applications: A Review. *J. Environ. Chem. Eng.* **2020**, *8* (5), No. 104175.
(22) Gan, D.; Wang, Z.; Li, X.; Zhou, J.; Dai, B.; Yang, L.; Xia, S. Green Synthesis of Bimetallic PdAg Alloy Nanoparticles Supported on Polydopamine-Functionalized Kaolin for Catalytic Reduction of 4-Nitrophenol and Organic Dyes. *Appl. Clay Sci.* **2023**, *244*, No. 107091.
(23) Shahriari, M.; Sedigh, M. A. H.; Shahriari, M.; Stenzel, M.; Zangeneh, M. M.; Zangeneh, A.; Mahdavi, B.; Asadnia, M.; Gholami, J.; Karmakar, B.; et al. Palladium Nanoparticles Decorated Chitosan-Pectin Modified Kaolin: Its Catalytic Activity for Suzuki-Miyaura Coupling Reaction, Reduction of 4-Nitrophenol, and Treatment of Lung Cancer. *Inorg. Chem. Commun.* **2022**, *141*, No. 109523.
(24) Asmare, Z. G.; Aragaw, B. A.; Atlabachew, M.; Dubale, A. A. Facile fabrication of Cu/kaolin nanocomposite as highly efficient heterogeneous catalyst for 4-nitrophenol reduction in aqueous solution. *Results Chem.* **2024**, *11*, No. 101836.
(25) Zhou, X.; Li, Y.; Xing, Y.; Liu, X.; Yu, X.; Yu, Y. Comparison of the Catalytic Properties of Au Nanoparticles Supported on Different Two-Dimensional Carriers. *J. Phys. Chem. Solids* **2020**, *142*, No. 109438.
(26) Li, C.; Sun, L.; Niu, J.; Reka, A. A.; Feng, P.; Garcia, H. Core-Shell Bi-Containing Spheres and $TiO_2$ Nanoparticles Co-Loaded on Kaolinite as an Efficient Photocatalyst for Methyl Orange Degradation. *Catal. Commun.* **2023**, *175*, No. 106609.
(27) Huang, X.; Wu, W. Research and Application of Graphite Oxide-Assisted High-Gravity Rotating Bed Liquid Phase Exfoliation of Kaolinite. *Chem. Pap.* **2023**, *77* (2), 745−755.
(28) Nasrollahzadeh, M.; Shafiei, N.; Baran, T.; Pakzad, K.; Tahsili, M. R.; Baran, N. Y.; Shokouhimehr, M. Facile Synthesis of Pd Nanoparticles Supported on a Novel Schiff Base Modified Chitosan-Kaolin: Antibacterial and Catalytic Activities in Sonogashira Coupling Reaction. *J. Organomet. Chem.* **2021**, *945*, No. 121849.
(29) Dong, W.; Zhang, J.; Zhuang, Z.; Zhong, J.; Zhang, J. Formulation of a Novel Anti-Human Oral Squamous Cell Carcinoma Supplement by Gold Nanoparticles-Kaolin Nanocomposite. *J. Exp. Nanosci.* **2022**, *17* (1), 138−149.
(30) Kim, T.; Lee, J.; You, M. J.; Song, C. H.; Oh, S.-M.; Moon, J.; Kim, J. H.; Park, M.-S. Enhanced Cycling Performance of a Li-Excess $Li_2CuO_2$ Cathode Additive by Cosubstitution Nanoarchitectonics of Ni and Mn for Lithium-Ion Batteries. *ACS Appl. Mater. Interfaces* **2023**, *15* (15), 18790−18799.
(31) Pei, N.; Liu, J.; Ma, H.; Chen, Z.; Zhang, P.; Zhao, J. Silver Copper Oxide Nanowires by Electrodeposition for Stable Lithium Metal Anode in Carbonate-Based Electrolytes. *ACS Sustainable Chem. Eng.* **2022**, *10* (21), 7196−7204.
(32) Gnanasekaran, L.; Pachaiappan, R.; Kumar, P. S.; Hoang, T. K. A.; Rajendran, S.; Durgalakshmi, D.; Soto-Moscoso, M.; Cornejo-Ponce, L.; Gracia, F. Visible Light Driven Exotic p (CuO) - n ($TiO_2$) Heterojunction for The Photodegradation of 4-Chlorophenol and Antibacterial Activity. *Environ. Pollut.* **2021**, *287*, No. 117304.
(33) Li, L.; Chen, X.; Quan, X.; Qiu, F.; Zhang, X. Synthesis of CuOx/$TiO_2$ Photocatalysts with Enhanced Photocatalytic Performance. *ACS Omega* **2023**, *8* (2), 2723−2732.
(34) Almarri, M. N.; Khalaf, M. M.; Gouda, M.; Heakal, F. E.-H.; Elmushyakhi, A.; Taleb, M. F. A.; El-Lateef, H. M. A. Surface, and Thermal Studies of Mixed Oxides Cupric Oxide (CuO), Lanthanum Oxide ($La_2O_3$), And Graphene Oxide for Dye Degradation from Aqueous Solution. *J. Mater. Res. Technol.* **2023**, *23*, 2263−2274.
(35) Asmare, Z. G.; Aragaw, B. A.; Atlabachew, M.; Wubieneh, T. A. Kaolin-Supported Silver Nanoparticles as an Effective Catalyst for the Removal of Methylene Blue Dye from Aqueous Solutions. *ACS Omega* **2023**, *8* (1), 480−491.
(36) Aragaw, T. A.; Angerasa, F. T. Synthesis and Characterization of Ethiopian Kaolin for The Removal of Basic Yellow (BY 28) Dye from Aqueous Solution as a Potential Adsorbent. *Heliyon* **2020**, *6* (9), No. e04975.
(37) Aimdate, K.; Srifa, A.; Koo-amornpattana, W.; Sakdaronnarong, C.; Klysubun, W.; Kiatphuengporn, S.; Assabumrungrat, S.; Wongsakulphasatch, S.; Kaveevivitchai, W.; Sudoh, M.; et al. Natural Kaolin-Based Ni Catalysts for $CO_2$ Methanation: On the Effect of Ce Enhancement and Microwave-Assisted Hydrothermal Synthesis. *ACS Omega* **2021**, *6* (21), 13779−13794.
(38) Kassa, A. E.; Shibeshi, N. T.; Tizazu, B. Z. Kinetic Analysis of Dehydroxylation of Ethiopian Kaolinite During Calcination. *J. Therm. Anal. Calorim.* **2022**, *147* (22), 12837−12853.
(39) Harish, B.; Alok, K. D.; Pankaj, K.; Purushottam, K. S.; Mohamed, M. A. Structure and Electrochemical Properties of CuO-ZnO Nanocomposite Produced by the One-Step Novel Discharge Process. *J. Taibah Univ. Sci.* **2023**, *17* (1), No. 2188017.
(40) Bharathi, P.; Wang, S.-F. Integration of Bismuth Sulfide/Functionalized Halloysite Nanotube Composite: An Electrochemical Tool for Diethofencarb Analysis. *Chemosphere* **2023**, *310*, No. 136834.
(41) Gvozdenko, A. A.; Siddiqui, S. A.; Blinov, A. V.; Golik, A. B.; Nagdalian, A. A.; Maglakelidze, D. G.; Statsenko, E. N.; Pirogov, M. A.; Blinova, A. A.; Sizonenko, M. N.; et al. Synthesis of CuO Nanoparticles Stabilized with Gelatin for Potential Use in Food Packaging Applications. *Sci. Rep.* **2022**, *12* (1), No. 12843.
(42) Vieillard, J.; Bouazizi, N.; Morshed, M. N.; Clamens, T.; Desriac, F.; Bargougui, R.; Thebault, P.; Lesouhaitier, O.; Le Derf, F.; Azzouz, A. CuO Nanosheets Modified with Amine and Thiol Grafting for High Catalytic and Antibacterial Activities. *Ind. Eng. Chem. Res.* **2019**, *58* (24), 10179−10189.
(43) Jenkins, M. J.; Phillips, M. A.; Xue, Z.-L. Solvatochromism of Cupric Chloride and Its Conversion to Copper Oxide. *J. Chem. Educ.* **2023**, *100* (12), 4772−4779.
(44) Kalidhasan, S.; Park, D.-G.; Jin, K. S.; Lee, H.-Y. Engineered Polymer-Clay-Copper Oxides Catalyst for The Oxidation and Reduction of Organic Molecules: Synergy of Degradation and Instinctive Interface Stability by Polymer Self-Healing Function. *Surf. Interfaces* **2023**, *39*, No. 102934.
(45) Khatoon, U. T.; Velidandi, A.; Rao, G. V. S. N. Copper oxide nanoparticles: Synthesis via chemical reduction, characterization,


https://doi.org/10.1021/acsomega.4c04029
*ACS Omega* 2024, 9, 48014−48031

antibacterial activity, and possible mechanism involved. *Inorg. Chem. Commun.* **2023**, *149*, No. 110372.
(46) Roopan, S. M.; Devi Priya, D.; Shanavas, S.; Acevedo, R.; Al-Dhabi, N. A.; Arasu, M. V. CuO/C nanocomposite: Synthesis and optimization using sucrose as carbon source and its antifungal activity. *Mater. Sci. Eng., C* **2019**, *101*, 404−414.
(47) Sharma, S.; Kumar, K.; Thakur, N.; Chauhan, S.; Chauhan, M. S. Eco-friendly Ocimum tenuiflorum green route synthesis of CuO nanoparticles: Characterizations on photocatalytic and antibacterial activities. *J. Environ. Chem. Eng.* **2021**, *9* (4), No. 105395.
(48) Karuppaiyan, J.; Mullaimalar, A.; Jeyalakshmi, R. Adsorption of Dyestuff by Nano Copper Oxide Coated Alkali Metakaoline Geopolymer in Monolith and Powder Forms: Kinetics, Isotherms, and Microstructural Analysis. *Environ. Res.* **2023**, *218*, No. 115002.
(49) Aditya, T.; Jana, J.; Singh, N. K.; Pal, A.; Pal, T. Remarkable Facet Selective Reduction of 4-Nitrophenol by Morphologically Tailored (111) Faceted $Cu_2O$ Nanocatalyst. *ACS Omega* **2017**, *2* (5), 1968−1984.
(50) Bekru, A. G.; Tufa, L. T.; Zelekew, O. A.; Goddati, M.; Lee, J.; Sabir, F. K. Green Synthesis of a CuO−ZnO Nanocomposite for Efficient Photodegradation of Methylene Blue and Reduction of 4-Nitrophenol. *ACS Omega* **2022**, *7* (35), 30908−30919.
(51) Roozitalab, A.; Kargari, A.; Soleimani, M. In *Effect of Calcination Temperature in Kaolin Membranes Structure*; 7th MEMTEK International Symposium 14−16 March 2023, on Membrane Technologies and Applications Istanbul, TÜRKİYE, 2023.
(52) Paul, A.; Weinberger, C.; Tiemann, M.; Wagner, T. Copper Oxide/Silica Nanocomposites for Selective and Stable H2S Gas Detection. *ACS Appl. Nano Mater.* **2019**, *2* (6), 3335−3338.
(53) Liu, Q.; Lyu, X.; Chen, Q.; Qin, Y.; Wang, X.; Li, C.; Fang, Z.; Bao, H. Fast Synthesis of Nanoporous Cu/Ag Bimetallic Triangular Nanoprisms via Galvanic Replacement for Efficient 4-Nitrophenol Reduction. *Nanoscale* **2024**, *16* (11), 5546−5550.
(54) Ye, H.; Hu, R.; Wang, Z.; Wang, J.; Zhou, S. Confinement Effect of Hollow Nanoreactors Enforcing the Formation of Pd−NixOy Hybrid Nanoparticles Inside for 4-Nitrophenol Catalytic Reduction. *Ind. Eng. Chem. Res.* **2023**, *63*, 288−295, DOI: 10.1021/acs.iecr.3c03396.
(55) Wang, Q.; Wei, Z.; Li, J.; Feng, D.; Feng, A.; Zhang, H. Hierarchical-Structured Pd Nanoclusters Catalysts x-PdNCs/CoAl-(O)/rGO-T by the Captopril-Capped Pd Cluster Precursor Method for the Highly Efficient 4-Nitrophenol Reduction. *ACS Appl. Mater. Interfaces* **2022**, *14* (24), 27775−27790.
(56) Abebe, B.; Tsegaye, D.; Sori, C.; Prasad, R. C. K. R.; Murthy, H. C. A. Cu/CuO-Doped ZnO Nanocomposites via Solution Combustion Synthesis for Catalytic 4-Nitrophenol Reduction. *ACS Omega* **2023**, *8* (10), 9597−9606.
(57) Ayagh, K.; Farrokhi, M.; Yang, J. K.; Shirzad-Siboni, M. Facile Provision of CuO-Kaolin Nanocomposite for Enhanced Sonocatalytic Removal of Cr(VI) from Aqueous Media. *Environ. Technol.* **2023**, *44* (3), 342−353.
(58) Liu, D.; Wang, Z.; Ma, Y.; Xu, C.; Zhou, S. Au−CuxOy Nanoparticles Encapsulated in Hollow Porous Silica Nanospheres as Efficient Catalysts for Nitrophenol Reduction. *ACS Appl. Nano Mater.* **2023**, *6* (1), 461−468.
(59) Kassem, A. A.; Abdelhamid, H. N.; Fouad, D. M.; Ibrahim, S. A. Catalytic Reduction of 4-Nitrophenol Using Copper Terephthalate Frameworks and CuO@C Composite. *J. Environ. Chem. Eng.* **2021**, *9* (1), No. 104401.
(60) Suresh, R.; Karthikeyan, N. S.; Gnanasekaran, L.; Rajendran, S.; Soto-Moscoso, M. Facile Synthesis of CuO/G-$C_3N_4$ Nanolayer Composites with Superior Catalytic Reductive Degradation Behavior. *Chemosphere* **2023**, *315*, No. 137711.
(61) Zhou, S.; Liu, C.; Jin, W.; Pan, L.; Jiang, Q.; Hu, Y.; Kong, Y. Density Functional Theory Study of Small Au Nanoparticles Anchored on the Inner Surface of Mesoporous Co3O4 for the Catalytic Reduction of 4-Nitrophenol. *ACS Appl. Nano Mater.* **2021**, *4* (5), 4763−4773.
(62) Jin, C.; Wang, D.; Wu, A.; Zhang, X.; Tian, C. The Synergy of Co-MoN-MnO on 2D Carbon Sheets for Effective Catalytic Hydrogenation. *Chem. Eng. J.* **2023**, *477*, No. 146822.
(63) Cheng, H.; Yang, Z.; Du, F.; Liu, H.; Zhang, Q.; Zhang, Y. Recyclable Ag/Halloysite Nanotubes/Polyvinyl Alcohol Sponges for Enhanced Reduction of 4-Nitrophenol. *Appl. Clay Sci.* **2022**, *223*, No. 106510.
(64) Kumar, S.; Dholakiya, B. Z.; Jangir, R. Covalent Organic Framework Impregnated with Silver and Copper Nanoparticles: An Advanced Approach for Catalytic Degradation of Organic Pollutants in Wastewater. *ACS Appl. Mater. Interfaces* **2024**, *16* (1), 1553−1563.
(65) Chatterjee, S.; Bhattacharya, S. K. Size-Dependent Catalytic Activity of PVA-Stabilized Palladium Nanoparticles in p-Nitrophenol Reduction: Using a Thermoresponsive Nanoreactor. *ACS Omega* **2021**, *6* (32), 20746−20757.
(66) Ayad, A. I.; Luart, D.; Dris, A. O.; Guénin, E. Kinetic Analysis of 4-Nitrophenol Reduction by "Water-Soluble" Palladium Nanoparticles. *Nanomaterials* **2020**, *10*, No. 1169.
(67) Mounir, C.; Ahlafi, H.; Aazza, M.; Moussout, H.; Mounir, S. Kinetics and Langmuir−Hinshelwood Mechanism for the Catalytic Reduction of Para-Nitrophenol over Cu Catalysts Supported on Chitin and Chitosan Biopolymers. *React. Kinet., Mech. Catal.* **2021**, *134* (1), 285−302.
(68) Hu, X.-D.; Shan, B.-Q.; Tao, R.; Yang, T.-Q.; Zhang, K. Interfacial Hydroxyl Promotes the Reduction of 4-Nitrophenol by Ag-based Catalysts Confined in Dendritic Mesoporous Silica Nanospheres. *J. Phys. Chem. C* **2021**, *125* (4), 2446−2453.
(69) Swathy, T. S.; Antony, M. J.; George, N. Active Solvent Hydrogen-Enhanced p-Nitrophenol Reduction Using Heterogeneous Silver Nanocatalysts@Surface-Functionalized Multiwalled Carbon Nanotubes. *Ind. Eng. Chem. Res.* **2021**, *60* (19), 7050−7064.


https://doi.org/10.1021/acsomega.4c04029
*ACS Omega* 2024, 9, 48014−48031